

# Fourier Photometric Analysis of Isolated Galaxies in the context of the AMIGA project

A. Durbala<sup>1\*</sup>, R. Buta<sup>1</sup>, J. W. Sulentic<sup>1</sup>, and L. Verdes-Montenegro<sup>2</sup>

<sup>1</sup>*Department of Physics and Astronomy, University of Alabama, Box 870324, Tuscaloosa, AL 35487-0324, USA*

<sup>2</sup>*Instituto de Astrofísica de Andalucía, CSIC, Apdo. 3004, 18080 Granada, Spain*

31 October 2018

## ABSTRACT

We present here the results of a Fourier photometric decomposition of a representative sample of  $\sim 100$  isolated CIG galaxies (Catalog of Isolated Galaxies; Karachentseva 1973) in the morphological range Sb-Sc. This study is an integral part of the AMIGA project. It complements the photometric analysis presented in our previous paper (Durbala et al. 2008) for the same sample of disk galaxies by allowing a description of the spiral structure morphology. We also estimate dynamical measures like torque strength for bar and spiral, and also the total nonaxisymmetric torque by assuming a constant M/L ratio, and explore the interplay between the spiral and bar components of galaxies. Both the length ( $l_{bar}$ ) and the contrast (e.g.  $A_{2b}$ ) of the Fourier bars decrease along the morphological sequence Sb-Sbc-Sc, with bars in earlier types being longer and showing higher contrast. The bars of Sb galaxies are  $\sim 3\times$  longer than the bars in Sc types, consistent with our previous study (Durbala et al. 2008). We find that the longer bars are not necessarily stronger (as quantified by the torque  $Q_b$  measure), but longer bars show a higher contrast  $A_{2b}$ , in very good agreement with theoretical predictions. Our data suggests that bar and spiral components are rather independent in the sense that the torque strengths of the two components are not correlated. The total strength  $Q_g$  is a very reliable tracer of the bar strength measure  $Q_b$ , the two quantities showing a very tight linear correlation. Comparison with a similar sample of disk galaxies (same morphological range) extracted from the OSUBGS (Ohio State University Bright Galaxy Survey; Eskridge et al. 2002) survey indicates that the isolated CIG/AMIGA galaxies host significantly longer Fourier bars and possibly show a different distribution of spiral torque  $Q_s$ . The Fourier analysis also revealed a potential case of counterwinding spiral structure (KIG 652/NGC 5768), which deserves further kinematic study. We find that  $m = 2$  (i.e. dominating two-armed pattern) is the most common spiral arm multiplicity among the sample of Sb-Sc CIG/AMIGA galaxies ( $\sim 40\%$ ),  $m = 2$  & 3 and  $m = 1$  & 2 are found in  $\sim 28\%$  and  $\sim 13\%$  of isolated galaxies, respectively.

**Key words:** galaxies: fundamental parameters; galaxies: photometry; galaxies: structure; galaxies: evolution; galaxies: spiral; galaxies: general

## 1 INTRODUCTION

This is our second study dedicated to a detailed photometric characterization of isolated galaxies in the context of the AMIGA (Analysis of the interstellar Medium of Isolated GALaxies) project<sup>1</sup>. Our first paper Durbala et al. (2008) presented a dual approach to characterize the properties of a representative sample of  $n \sim 100$  Sb-Sc isolated galaxies: bulge/disk/bar decomposition and CAS (Concentration/Asymmetry/Clumpiness) parametrization. The main goal was to explore morphological type differences

using quantitative structural (photometric) analysis. In that context we quantified structural properties of galaxies thought to be least influenced by environment ( $\sim$  zero nurture). Since one expects that environment almost certainly increases “dispersion” in virtually all galaxy measures, we wanted to constrain the best estimates of “intrinsic dispersion” ( $\sim$  pure nature).

So far we find: i) extreme bias towards spirals (few E+S0; Sulentic et al. 2006), ii) bias to intermediate-late type spirals, with a clear dominance of Sb-Sc morphological types (Sulentic et al. 2006), iii) the majority of CIG/AMIGA disk galaxies host pseudobulges (Durbala et al. 2008), iv) the core sample of CIG/AMIGA isolated galaxies (Sb-Sc types) tends to host larger bars and shows lower concentration and asymmetry measures than galaxy samples

\* E-mail: adriana.durbala@ua.edu

<sup>1</sup> <http://www.iaa.es/AMIGA.html>

of similar morphological classification selected without isolation criteria (Durbala et al. 2008).

However, neither approach in Durbala et al. (2008) was sensitive to the spiral arm morphology, which is intimately connected to the global galactic morphology. This paper presents a 2D Fourier decomposition/analysis of the same sample explored in that previous paper. The present study offers a complementary description not only by incorporating the structural properties of the spiral arms, but also allowing for dynamical measures (i.e. gravitational torque) for bars, spiral arms and total (bar+spiral) nonaxisymmetric components. We emphasize that these dynamical measures (see §§§ 3.1.2) will be referred herein as “strength”. There are studies (e.g. Athanassoula 2003) where other kind of measures defined in terms of relative Fourier amplitudes are called “strength”. Such parameters are similar to what would be referred in our context as “contrast” (see § 4).

In the context of the AMIGA project a similar Fourier decomposition technique was employed by Verley et al. (2007b) for a different sample of isolated galaxies spanning the full range of morphological types later than S0/a. That study explored the dynamical influence of bars on star formation properties.

The representative collection of isolated Sb-Sc CIG/AMIGA galaxies we have examined in the present paper (and also in Durbala et al. 2008) constitutes a valuable control sample to test the predictions of theoretical models regarding the coevolution and the interplay between various galactic components. The goal is to compare our results of the Fourier analysis for our sample of isolated galaxies with measures from samples selected without isolation criteria. The main question is whether we could reveal the environmental influence on the morphology and dynamics of spiral galaxies. We would also like to present a census of the spiral pattern morphology, i.e. we evaluate the frequency of occurrence of one-, two- or three-armed pattern morphology amongst our sample.

This paper is organized as follows: § 2 presents our sample, § 3 offers a detailed description of the data reduction and the Fourier decomposition, § 4 is dedicated to the analysis of the parameters provided by Fourier decomposition. § 5 discusses the results of this study and § 6 outlines the most important conclusions. Throughout the paper we use  $H_0 = 75 \text{ km s}^{-1} \text{ Mpc}^{-1}$ .

## 2 SAMPLE

Our isolated galaxy sample is drawn from the Catalog of Isolated Galaxies (CIG; Karachentseva 1973). We focus on Sb-Sc morphological type, since they represent the bulk (63%) of all isolated AMIGA galaxies (Sulentic et al. 2006). The sample selection was described in detail in Durbala et al. (2008), where we studied galaxies that have inclinations less than  $\sim 70^\circ$  and have i-band images available in the Sloan Digital Sky Survey (SDSS-DR6). In our present study we exclude one galaxy (KIG 907) because we cannot get reliable Fourier measures. Therefore, the statistical analysis herein will focus on a sample of  $n=93$  galaxies.

## 3 DATA REDUCTION

The SDSS i-band frames we use are flat-field, bias, cosmic ray and pixel-defect corrected (Stoughton et al. 2002). Foreground stars were removed from the images using IRAF task IMEDIT. Sky fitting and subtraction were accomplished using IRAF task IMSURFIT. The  $aa$ ,  $kk$  and  $airmass$  coefficients (zeropoint, extinction co-

efficient and airmass) from the SDSS TsField files were used to perform the photometric calibration<sup>2</sup>. The surface brightness zeropoint was calculated using the following formula:  $2.5 \times \log(exptime \times 0.396^2) - 2.5 \times 0.4 \times (aa + kk \times airmass)$ , where an exposure time  $exptime$  of 53.907 seconds and a pixel size of  $0''.396$  were used.

### 3.1 Fourier Decomposition

The observed light distribution in a deprojected galaxy image can be expanded in Fourier series:

$$I(r, \phi) = I_0(r) + \sum_{m=1}^{\infty} I_{mc}(r) \cos m\phi + \sum_{m=1}^{\infty} I_{ms}(r) \sin m\phi$$

or

$$I(r, \phi) = I_0(r) + \sum_{m=1}^{\infty} I_m(r) \cos[m(\phi - \phi_m)],$$

where  $I_0(r)$  is the azimuthally-averaged intensity in a circular annulus at a radius  $r$  in the galaxy plane,  $I_{mc}$  and  $I_{ms}$  are the cosine and sine amplitudes, respectively and  $\phi_m$  is the phase for each Fourier component  $m$ .

The  $I_0(r)$  ( $m=0$ ) term defines the axisymmetric background, and has contributions from all components, including the bulge, disk, bar, and spiral arms. The bar and the spiral arms are non-axisymmetric components, whose Fourier description requires a 2D treatment in both radial and angular polar coordinates. Our 2D analysis differs from standard 2D Fourier transforms (e.g. Considered & Athanassoula 1988; Puerari & Dottori 1992) in that we do not transform the whole 2D image into its frequency components, but operate on 1D azimuthal profiles at successive radii, and use averages to derive the radial amplitudes of different  $m$  components.

The Fourier  $I_m$  amplitudes are expressed by:

$$I_m = \sqrt{I_{mc}^2 + I_{ms}^2}$$

#### 3.1.1 Bar-Spiral Separation

The galaxies have been deprojected using the IRAF task IM-LINTRAN. The orientation parameters (mean orientation angle and axial ratio) of the disk were input parameters in this IRAF routine. The mean orientation angle (of the galaxy’s major axis) is defined relative to an XY plane overlapping the image of a galaxy, centered on the galaxy’s center, whose identification is explained in section 3 of Durbala et al. (2008). It is measured counterclockwise relative to the positive x-axis. It is provided by the BUDDA code<sup>3</sup> (BULge/Disk Decomposition Analysis; de Souza, Gadotti & dos Anjos 2004). We make available the orientation measures in Table 1. The axial ratio is tabulated as an inclination measure  $i$ ,  $\cos(i) = b/a$  in our previous photometric study Durbala et al. (2008).

We assume that the galaxy disk is circular and the deprojection is performed about the major axis of the galaxy. For deprojection purposes we are forced to apply a simplifying approach; in the “face-on” display of the galaxy the bulge should be as close as possible to a circular shape. Thus we have three different cases: a)

<sup>2</sup> <http://www.sdss.org/dr6/algorithms/fluxcal.html>

<sup>3</sup> <http://www.mpa-garching.mpg.de/~dimtiri/budda.html>

in most situations, the deprojection procedure automatically leads to a circularly shaped bulge, b) in some cases the bulge is already circular in the original image (prior to deprojection), in which case we subtract the bulge model given by the BUDDA decomposition code first (see Durbala et al. 2008, we then deproject the bulge-subtracted image and finally we add back the bulge model and c) if neither before nor after deprojection the bulge appears circular we outline the following recipe: 1) using BUDDA we force a circular bulge model fit to the SDSS reduced image (before deprojection), even though the bulge may not appear circular; 2) we subtract the bulge model from the SDSS image; 3) we deproject the resultant image (which is now bulge-less); 4) we add back the adopted BUDDA bulge model from step 1 to the “face-on” bulgeless deprojected image from step 3; 5) we take an average of the image produced in step 4 and the image obtained by directly applying the aforementioned method (a), when an elongated bulge appears after deprojection. We emphasize that the averaging process affects only the bulge component within the image. The resultant image in step 3 and the deprojected image (method (a)) are basically identical outside the bulge region. In Table 1 (column 3) we indicate the bulge deprojection method employed for each galaxy.

We are aware that the true morphology/geometry of bulges could be far more complicated and that a round/axisymmetric bulge may be an oversimplification. Nonetheless, our assumptions are beneficial for two reasons: i) they do not artificially create ovals by deprojection and ii) do not severely interfere with the study of spiral arm morphology within galaxies. The fact that case (a) was typical for the large majority of our galaxies (70%) gives some support to our simplifying assumptions about the bulge.

The first step of the Fourier analysis is bar-spiral separation. A bar is a feature that is dominated by even Fourier terms. The bar is separated by fitting a single or a double Gaussian function in the bar region (Buta et al. 2005). In a few cases neither of the two models appear satisfactory so the symmetry assumption is used, i.e. the left side of the profile can be mirrored. Sometimes there is only a single maximum intensity (e.g. Figure 3,  $m=6$  term for KIG553 explained in the next paragraphs), so the relative Fourier intensities decrease from the peak in a similar way as they rose to that peak (Buta, Block & Knapen 2003). In other cases the “mirror-axis” falls in between two peaks (e.g. Figure 3,  $m=2$  and  $m=4$  terms). Sometimes (but not always) a profile produced by our symmetry assumption can closely mimic a single or a double-Gauss profile. Deciding the best solution (Gaussian, double Gaussian or “mirroring”/symmetry assumption) is an iterative process driven by the visual check for minimum residuals in the bar-subtracted image. Typically under- or over-subtraction of the bar model would show as extra- or deficit-light patches spatially coinciding with the outer parts of the bar.

For all cases the first 20 terms in the Fourier expansion retain virtually all photometric information about the galaxy, thus only these first 20 terms are used to model the bar and galaxy light distribution. Beyond  $m=20$  we practically reach the background noise level.

In simple terms the bar spatial extent could be seen as the radius over which the bar light distribution model is non-vanishing. The bar is defined as the sum of model fits in all even Fourier terms over its spatial extent.

The first six figures show examples of bar fitting and bar-spiral separation for three galaxies: KIG 550, 553 and 719, illustrating all three possible choices for bar fitting explained (single Gaussian, double Gaussian or symmetry assumption with no attempt to describe analytically the profile in this latter case).

- **KIG 550:** Figure 1 shows the bar fitting for galaxy KIG 550. The left panels of Figure 1 display the relative Fourier intensities  $I_m/I_0$  for the first six even Fourier terms from  $m=2$  to  $m=12$  (solid line) as a function of radius. The cross symbols show the mapping of the bar. The last term used in the Fourier expansion to describe the bar is  $m=10$ . The bar was fitted with a Gaussian in all even Fourier terms from  $m=2$  to  $m=10$ . The right panels of Figure 1 present the phase profiles  $\phi_m$  for the same first six even Fourier terms ( $m=2$  to  $m=12$ ).

The output images obtained from the Fourier decomposition of this galaxy are shown in Figure 2. The upper left panel displays the original deprojected image. “M=0-20 SUM” image is the sum all even and odd Fourier terms from  $m=0$  to  $m=20$ . This image can be regarded as a “Fourier-smoothed” version of the original image (Buta, Block & Knapen 2003). The “BAR + DISK” image is the sum of the bar image (e.g. sum of all even Fourier terms within the bar limits that have a non-negligible contribution) and  $m=0$  image (i.e. axisymmetric light distribution). The “SPIRAL + DISK” image is the “M=0-20 SUM” image minus the bar image.

- **KIG 553:** Figure 3 presents the bar fitting for galaxy KIG 553. The left panels show the relative Fourier intensity amplitudes  $I_m/I_0$  for the first even Fourier terms up to  $m=20$  (solid line). The mapping of the bar is shown with cross symbols. The right panels of Figure 3 present the phase profiles  $\phi_m$  for the same first ten even Fourier terms ( $m=2$  to  $m=20$ ). In this example the last term used in the Fourier expansion to describe the bar is  $m=18$ . For the first 5 even Fourier terms ( $m=2$  to  $m=10$ ) the symmetry assumption is used and for the next even terms ( $m=12$  to  $m=18$ ) the bar is modeled with a Gaussian (Figure 3 - left panels). The fact that the phase is not constant within the inner  $5''$  is a deprojection effect that we could not totally eliminate.

The output Fourier images are shown in Figure 4. The designations are the same as in Figure 2.

- **KIG 719:** This is one of the two galaxies in our sample that harbors an AGN (Seyfert1 nucleus). The AGN component was fitted by the BUDDA code and then subtracted from the original image prior to proceed to the Fourier decomposition. The bar was fitted with two Gaussians. The last term included in the Fourier expansion to model the bar was  $m=10$ . The left panels of Figure 5 show the relative Fourier intensity amplitudes  $I_m/I_0$  as a function of radius for the first six even Fourier terms from  $m=2$  to  $m=12$  (solid line). The bar fitting is indicated with cross symbols. The phase profiles  $\phi_m$  as a function of radius for the same first six even Fourier terms ( $m=2$  to  $m=12$ ) are displayed in the right panels of Figure 5.

The Fourier images obtained after bar-spiral separation are displayed in Figure 6, the designations being the same as for Figure 2.

### 3.1.2 Estimation of Bar, Spiral and Total Strengths

We employ the gravitational torque method (Sanders & Tubbs 1980; Combes & Sanders 1981; Buta & Block 2001) to derive the bar, spiral and total strengths for the galaxies in our sample. A constant mass-to-light ratio is assumed. The procedure is described in detail in Buta, Block & Knapen (2003). The vertical disk scale-height is inferred from the radial scalelength following the galaxy morphological type dependent prescription from de Grijs (1998).

The relative strength of the perturbation is calculated at each

radius  $r$  in the plane of the galaxy as a force ratio:

$$Q_T(r) = \frac{|F_T(r, \phi)|_{max}}{\langle |F_R(r, \phi)| \rangle},$$

where  $|F_T(r, \phi)|_{max}$  and  $\langle |F_R(r, \phi)| \rangle$  are the maximum tangential force and the azimuthally averaged radial force, respectively at a radius  $r$ . The strength is defined as the maximum of the function  $Q_T(r)$ .

The bar strength ( $Q_b$ ) is calculated using the ‘‘BAR + DISK’’ image, which includes all even Fourier terms contributing to the bar plus the  $m=0$  term, i.e. the mean axisymmetric background. The spiral arms strength ( $Q_s$ ) is determined from the ‘‘SPIRAL + DISK’’ image. The total strength of the galaxy ( $Q_g$ ) is derived from the ‘‘M=0-20 SUM’’ image (so-called ‘‘Fourier-smoothed’’ image). The total strength includes both the bar and the spiral structure. In a strongly barred galaxy  $Q_g \approx Q_b$ , while in a galaxy where the spiral dominates  $Q_g \approx Q_s$ .

Figures 7, 8 and 9 present the relative strength of the gravitational perturbation/torque  $Q_T(r)$  as a function of radius for KIG 550, KIG 553 and KIG 719, respectively. Bar strength  $Q_b$ , spiral strength  $Q_s$  and total strength  $Q_g$  are indicated on the figures as absolute maxima.

#### 4 FOURIER ANALYSIS

Table 1 includes the Fourier-derived parameters for our sample. The designations of each column are as follows: (1) galaxy name, (2) orientation angle (see §§§ 3.1.1), (3) bulge deprojection method (see §§§ 3.1.1), (4) total strength  $Q_g$ , (5) bar strength  $Q_b$ , (6) spiral arms strength  $Q_s$ , (7)  $A_{2b}$ , (8)  $A_{4b}$ , (9)  $A_{6b}$ , (10) Fourier bar length and (11) radius of maximal bar torque  $r(Q_b)$ .

We define  $A_{mb}$  as the maximum of the relative Fourier intensity amplitudes:

$$A_{mb} = \left( \frac{I_m}{I_0} \right)_{max},$$

where  $m$  is an even integer number. The  $A_{mb}$  indicates the contribution of the non-axisymmetric component relative to the axisymmetric background, thus one may see it as a ‘‘contrast’’ measure. Hereafter we would use it as such.

For practical reasons the adopted definition for bar length  $l_{bar}$  is not fully identical to the bar spatial extent described in §§§ 3.1.1. The length of the bar  $l_{bar}$  is the spatial (radial) extent where the bar model fit (section §§§ 3.1.1) is non-zero AND the phase is nearly constant (Laurikainen et al. 2004; Laurikainen, Salo & Buta 2005) in both  $m=2$  and  $m=4$  terms. Taken independently, for the large majority of cases, the two criteria are in agreement within  $2\sigma$  uncertainty. By ‘‘nearly constant’’ we mean that we typically allow for a maximum of 10 degrees variation ( $\pm 5$  degrees relative to an average). This provides a rather conservative estimate that allows us to have common grounds with the comparison sample presented later in §§ 4.7.

We find a very tight correlation (correlation coefficient 0.95) between the Fourier  $l_{bar}$  and the radius where the bar torque gets the maximal value  $Q_b$ . It is shown in Figure 10 along with the best linear regression fit. The slope of the linear fit is 1.42. This is in good agreement with the empirical relation between  $r(0.25A_{4b})$  (i.e., the radius where the  $I_4/I_0(r)$  profile declines to 25% of its maximum  $A_{4b}$ ) and  $r(Q_b)$  proposed by Buta et al. (2009). That reference reports that  $r(0.25A_{4b})$  provides a very good approximation for the visual bar radius.

We checked whether our sample is affected in terms of Fourier measures by biases related to inclination or redshift. We found no correlations between the Fourier derived parameters and inclination or redshift.

Table 2 presents mean/median measures of  $Q_g$  and  $Q_s$  in three morphological bins Sb-Sbc-Sc for the whole sample of  $N=93$  galaxies. Table 3 provides average values for the strength measures  $Q_g$ ,  $Q_s$  and  $Q_b$  along with the bar contrast  $A_{2b}$  and bar length  $l_{bar}$  for the sample of  $N=46$  barred galaxies split in the same three bins. Table 4 gives average  $Q_g = Q_s$  values for  $N=47$  non-barred galaxies.

#### 4.1 Identifying Bars with the Fourier Decomposition

In our previous paper (Durbala et al. 2008) 55 out of 93 galaxies in the sample were visually classified as SAB or SB. The bulge-disk-bar decomposition code BUDDA could fit a bar for only 48 out of the 55 SAB/SB galaxies. Within the current approach the essence of a Fourier bar definition relies on the constancy of phase. This may lead to some discrepancy between what Fourier decomposition defines as the bar and what our visual evaluation (or the BUDDA decomposition code) identifies as the bar. The most sensitive (i.e. uncertain) cases are SAB galaxies for which an oval rather than a clear bar is assigned visually (or with the BUDDA code), but the phase is not constant in the Fourier terms  $m=2$  and  $m=4$ . Part of the discrepancy could be caused by the deprojection. The original visual classification and the BUDDA-based decomposition are both performed without any deprojection of images, while Fourier decomposition requires deprojected images. Actually we find that ten SAB and one SB galaxies do not show a constant phase in the bar region in  $m=2$  and  $m=4$  Fourier terms, therefore they do not have a Fourier bar component. We would like to point out another source of uncertainty when deciding visually or with a code like BUDDA on the presence/absence of a bar. In galaxy KIG 652, the Fourier decomposition reveals two widely open spiral arms in the inner region that mimic a bar in the original image and thus could be mistakenly classified as barred. Galaxy KIG 712 shows in its original image an elongated ring-like structure that appears decoupled in terms of orientation from the large disk of the galaxy. The Fourier decomposition assimilates this structure to a Fourier-bar associated with a constant phase. It is not clear that the bar structure in this case is real.

The Fourier decomposition offers an additional advantage when it comes to identifying bars in galaxies that show no clear indication of such feature by simple visual inspection. Two galaxies that we initially classified SA are now found to have a bar/oval in the Fourier analysis, i.e. Fourier bars, as indicated by both the large relative amplitude in the even terms  $m=2,4,6$  and the constancy of phase. All in all 46 out of 93 galaxies in our sample have a bar/oval component separated by the Fourier analysis.

#### 4.2 Total Nonaxisymmetric Strength

Figure 11 presents the distribution of the total strength for the galaxies in our sample. Mean ( $\pm$  standard deviation) and median for the distribution are indicated on the plot. Galaxies in our sample cover a wide range in total strengths between 0.05 and 0.55 with the bulk of the sample concentrated between 0.05 and 0.3.

Table 2 presents average values (mean and median) for the spiral and total strength measures for all galaxies in our sample. Total strength  $Q_g$  decreases from Sb to Sbc and then it slightly increases from Sbc to Sc morphological types. Tables 3 and 4 show

average strength parameters for barred and non-barred galaxies, respectively. Barred galaxies show total strength  $Q_g \sim 1.5 \times$  larger than non-barred galaxies. This trend is seen for all morphological types in our examined range Sb-Sbc-Sc.

### 4.3 Bar Strength and Bar Contrast

Figure 12 presents the distribution of the bar torque strength for the barred galaxies (N=46 Fourier bars) in our sample. Mean ( $\pm$  standard deviation) and median for the distribution are indicated on the figure. Barred galaxies in our sample show a wide spread in bar strength between 0.05 and 0.55 with the majority in the range 0.15-0.25. However, on average, there is no significant difference between the three morphological groups Sb-Sbc-Sc in terms of bar strength (Table 3).

The average values of the maximum relative Fourier amplitudes in  $m = 2, 4$  and  $6$  Fourier terms ( $A_{2b}, A_{4b}$  and  $A_{6b}$ ) show a clear decline along the morphological range we focus on, with Sb types showing the largest values and Sc types the lowest. In Table 3 we show only  $A_{2b}$  average values in each morphological bin, but not the other two bar contrast terms for  $m=4$  and  $m=6$  because a few barred galaxies have a negligible bar Fourier contribution from the 4th and/or 6th term.

Figures 13(a)-(c) show the relation between bar strength  $Q_b$  and the maximum relative Fourier amplitudes  $A_{2b}, A_{4b}$  and  $A_{6b}$ , respectively. The three morphological types Sb-Sbc-Sc are displayed with different symbols (see figure's legend). We see a clear morphological separation in each panel, largely driven by  $A_{2b}, A_{4b}$  and  $A_{6b}$ . Sb galaxies tend to have larger maximum relative Fourier amplitudes while Sc seem to show smaller values. Sb galaxies almost always have values of  $Q_b$  larger than  $\approx 0.15$ . Sbc-Sc galaxies seem to show a wider range in  $Q_b$ , including values smaller than 0.15. For the plot of  $Q_b$  versus  $A_{2b}$  the best (linear) correlation coefficient is obtained for Sbc and Sc galaxies ( $R=0.89$  and  $R=0.85$ , respectively) while Sb galaxies have  $R=0.47$ . We masked one point (KIG 339) when we calculated the correlation coefficient for Sbc galaxies. Although visual morphological classification retains some subjectivity, the separation seen in plots like those presented in Figure 13 may be regarded as an indirect confirmation of the robustness of classification. Probably KIG 339 should have been classified as an Sb instead of Sbc, since it shows as up in all panels in the space occupied by Sb galaxies.

### 4.4 Spiral Arm Strength

Figure 14 shows the histogram distribution of the spiral strengths  $Q_s$  for our sample. Mean ( $\pm$  standard deviation) and median of the distribution are indicated on the plot. Galaxies in our sample display spiral strengths between 0.05 and 0.45 with rare cases of  $Q_s > 0.3$ .

Sc galaxies appear to show the strongest spiral structure (Table 2), the effect being even more noticeable when restricting the comparison to the barred subsample (Table 3). In non-barred spiral galaxies we don't see any clear trend for  $Q_s$  (see Table 4). We should also point out that barred and non-barred galaxies seem to show similar spiral strengths (Table 3 versus Table 4), in contrast to the total strength  $Q_g$  where we noted a systematic effect, with barred galaxies being  $1.5 \times$  stronger within each morphological bin along the Sb-Sbc-Sc sequence (see section §§ 4.2)

### 4.5 The Interplay between Bar and Spiral Components

Figure 15(a) shows the spiral strength as a function of bar strength for the galaxies in our sample. The three morphological types are indicated with different symbols (see figure's legend). No clear correlation between spiral and bar strength is seen. Figure 15(b) shows such a plot of spiral strength  $Q_s$  as a function of  $A_{2b}$ . Again no correlation between bar contrast and spiral strength is revealed, but now the morphological segregation between earlier and later types is evident. The clearest separation between Sb and Sc types is enhanced here by the fact that Sb types show on average the largest  $A_{2b}$  and lowest  $Q_s$  values, while Sc galaxies show the opposite tendency (Table 3). The morphological separation seen in panel b still holds if one tries to plot  $Q_s$  versus  $A_{4b}$  or  $Q_s$  versus  $A_{6b}$  (not shown here).

Figure 16(a) presents the total strength of the galaxy as a function of the bar strength for the barred galaxies in our sample (N = 46). The three morphological types are indicated with different symbols. The solid line represents the best linear fit (correlation coefficient  $R=0.96$ ). The two parameters are very well correlated, which is not the case for  $Q_g$  and  $Q_s$  in Figure 16(b). The two panels of Figure 16 emphasize the noise in bar-spiral separation. The strong correlation between total and bar strength indicates that the former is a good tracer of the latter. We find the following linear relation:

$$Q_g = 0.829 \cdot Q_b + 0.079$$

It is important to note that for the barred galaxies (Table 3)  $Q_b$  is systematically larger than  $Q_s$  within each morphological segment Sb-Sbc-Sc. In most barred galaxies the total torque is dominated by the bar contribution ( $Q_b > Q_s$  in 34 out of 46 barred galaxies).

### 4.6 The Length of Fourier Bars

Figure 17 presents the distribution of bar lengths for the N=46 barred galaxies in our sample. Practically all barred galaxies in our sample display bar lengths (radii) less than 10 kpc. The last column of Table 3 gives the average values of the bar lengths for the three morphological types represented in our sample Sb-Sbc-Sc. The size of the bar decreases by almost a factor of  $\approx 3$  from Sb to Sc galaxies. The decreasing trend in bar sizes is similar to that reported in our previous paper (Durbala et al. 2008), with the exception that bar sizes were found to decrease by a factor of 2 from Sb to Sc galaxies in that study. In Durbala et al. (2008) bar sizes were determined from bulge-disk-bar decomposition (BUDDA code) of the original images (without deprojecting them).

Figure 18 presents bar strength and bar contrast in the  $m = 2$  term (panel a and b, respectively) as a function of the Fourier bar size. Panel a clearly indicates that the longer bars are not necessarily the stronger ones. Panel b on the other hand shows a significant linear correlation (correlation coefficient  $R=0.68$ ) and tells us that the longer the bar, the more prominent it appears in the sense that it shows a bigger contrast in the  $m=2$  Fourier term. The clear correlation shown in panel b is preserved even when replacing the absolute bar size  $l_{bar}$  with the normalized quantity  $l_{bar}/a_{25}^i$  (linear correlation coefficient  $R=0.69$ ), where  $a_{25}^i$  is the galactic disk semimajor axis of the 25 mag arcsec $^{-2}$  isophote in the SDSS i-band. The morphological separation is evident in both panels b and c with earlier Hubble types having longer and larger relative Fourier amplitude bars in  $m=2$  (see also Elmegreen et al. 2007).

#### 4.7 Comparison with the OSU sample

In this subsection we compare our Fourier-derived measures for our isolated sample with similar measures for a sample selected without isolation criteria. The best comparison sample available at this time is the Ohio State University Bright Galaxy Survey (hereafter OSU; Eskridge et al. 2002). Total strengths  $Q_g$  for the OSU sample are available in Laurikainen et al. (2004) and the bar and spiral strengths  $Q_b$  and  $Q_s$  are presented in Buta et al. (2005). We note that the Fourier measures for the OSU sample are derived from H-band (near-IR) images. The OSU sample has a comparable number of Sb-Sc galaxies (N=92 galaxies with Fourier-derived measurements, out of 116 morphologically classified in this narrow range). We adopted the RC3 catalogue (de Vaucouleurs et al. 1991) morphological classification for the OSU sample. Both our sample and the 92 OSU galaxies show a similar absolute magnitude  $M_B$  distribution, ranging from -22 to -18 with a mean/median of -20.4). The number of galaxies in each morphological type bin Sb-Sbc-Sc is also very similar to our sample (25-32-35). We defined a subsample of N=60 barred galaxies from the N=92 OSU Sb-Sc sample considering that a galaxy is classified as “barred” if it shows a Fourier bar, i.e. a constant phase in the  $m=2$  and  $m=4$  terms. The Fourier bar length measurements for the OSU sample are tabulated in Laurikainen et al. (2004).

Figure 19(a) presents the histogram distribution of the total strengths for the OSU Sb-Sc galaxies (N=92). Mean and median values are shown on the graph. The  $Q_g$  distributions of the OSU and our isolated sample (recall Figure 11) are very similar, with only three OSU galaxies exceeding  $Q_g \sim 0.55$ . A Kolmogorov-Smirnov (KS) test<sup>4</sup> gives a 47.6% probability of the null hypothesis (i.e., the two samples are drawn from the same parent population).

Figure 19(b) displays the distribution of the bar strengths  $Q_b$  for OSU Sb-Sc barred galaxies (N=60). Again we find that the  $Q_b$  distributions of the OSU and our isolated sample (recall Figure 12) are very similar in terms of the range covered and average values, with only two OSU galaxies exceeding  $Q_b \sim 0.55$ . We note however that the CIG/AMIGA sample of barred galaxies shows a strong concentration (50%) in the range  $Q_b=0.15-0.25$ , while the OSU barred sample includes only  $\sim 25\%$  in the same interval. A KS test gives a 73.1% probability of the null hypothesis. The similarity between the bar strength distribution in isolated galaxies and OSU disk galaxies is reported also in Verley et al. (2007b) based on a comparison that included a broader morphological range, i.e. later than S0/a.

The spiral arm strength  $Q_s$  distribution for the whole OSU Sb-Sc galaxies (N=92) is presented in panel c of Figure 19. Only two OSU galaxies show  $Q_s$  in excess of 0.35. A KS test gives a 0.4% probability of the null hypothesis, which may indicate a significant difference between the CIG/AMIGA sample (Figure 14) and OSU galaxies in terms of spiral strength measure.

Figure 19(d) shows the histogram distribution of the Fourier bar length  $l_{bar}$  for the OSU sample of N=60 barred galaxies. This distribution appears significantly different from that for the CIG/AMIGA sample (Figure 17); the OSU sample is clearly lacking large bars. A KS test confirms that the two distributions are different, giving a 0.2% probability of the null hypothesis.

A more detailed comparison between the CIG/AMIGA and OSU samples is possible if one focuses on the narrow morphological types (bins) Sb-Sbc-Sc. We present average values of the Fourier decomposition measures for the OSU sample in Tables 5, 6

and 7 following the framework illustrated in Tables 2, 3 and 4 for the CIG/AMIGA sample, which facilitates a straightforward parallel analysis<sup>5</sup>.

We can summarize several differences between the isolated and the OSU samples:

i) Comparing  $Q_s$  for all (barred+nonbarred) we note that the isolated Sb and Sc galaxies show larger average values relative to OSU Sb and Sc galaxies, but the Sbc types show rather similar  $Q_s$  measures (Tables 2 and 5).

ii) In Table 2 (isolated galaxies) we observe a decline for the average total strength  $Q_g$  from Sb to Sbc, but for the OSU sample we see a reversed trend from Sb to Sbc (Table 5; see also Figure 14 in Buta, Laurikainen & Salo 2004).

iii) Isolated barred galaxies (Table 3) show an almost constant  $Q_b$  for all three morphological bins, while in the OSU sample (Table 6) there is a slightly increasing trend from Sb through Sc.

iv) Isolated barred Sb galaxies (Table 3) show larger spiral strength  $Q_s$  measures than their OSU counterpart (Table 6). Sbc and Sc barred galaxies are similar in terms of average  $Q_s$  in the two samples.

v) The average  $Q_g$  for Sb isolated barred galaxies is larger than the average  $Q_g$  for the barred Sb from OSU (Tables 3 and 6). The OSU galaxies show an increasing trend along the Sb-Sbc-Sc sequence, but the isolated barred galaxies show a dip at Sbc types.

vi) In terms of bar contrast measure  $A_{2b}$  the isolated sample shows a clear decline (about a factor of two) along the Sb-Sbc-Sc morphological sequence with a larger difference between Sb and Sbc (Table 3). The OSU sample shows very similar  $A_{2b}$  averages for Sb and Sbc bins and only a modest decline (if any) between Sbc and Sc types (Table 6).

vii) The Fourier bar length  $l_{bar}$  for the isolated sample shows a decreasing trend from Sb through Sc, overall by about a factor three between Sb and Sc (Table 3). However, the OSU sample shows only slightly shorter bars for the latest types Sc, while the Sb and Sbc are on average much more similar.

viii) Intercomparison by morphological bins reveals that the isolated and OSU Sb barred galaxies show similar average  $A_{2b}$  values (Tables 3 and 5), but for Sbc and Sc types OSU galaxies show larger values. For Sb and Sbc types, the bars in isolated galaxies are systematically longer, but in the case of Sc types there is no significant difference. As shown in Figure 20 in both samples CIG/AMIGA and OSU there is a positive trend between the bar contrast and its size. The isolated barred galaxies apparently show a different scaling relation between  $l_{bar}$  and  $A_{2b}$  than the barred galaxies from the OSU sample within the same morphological interval  $T=3-5$ . For a similar  $l_{bar}$  the isolated galaxies show a lower contrast. However this difference can be attributed to the fact that we perform our analysis on SDSS i-band images and OSU Fourier measures are extracted from H-band near-IR images. It is well known that near-IR images, much less affected by extinction and good tracers of old stellar populations, could reveal more clearly the presence/absence of bars. This is also reflected by the significantly larger number of barred galaxies in the comparison OSU sample (60 out of 92).

<sup>5</sup> We should point out that in Table 7,  $Q_g$  is not equal to  $Q_s$  (as was the case for the isolated galaxies in Table 4). This is due to a slightly different approach of the aforementioned references that provide the Fourier parametrization for the OSU sample; the authors include a bar component in all galaxies, thus for some galaxies they report a nonvanishing  $Q_b$  (typically smaller than 0.05) even though visually one cannot unambiguously identify a bar.

#### 4.8 Spiral Arm Multiplicity

Using the  $I_{mc}$  and  $I_{ms}$  amplitudes we could reconstruct the images of the individual  $m$  Fourier terms. For example, the  $m=1$  image would be given by  $I_{1c}(r) \cos \phi + I_{1s}(r) \sin \phi$  and the  $m=2$  image would be given by  $I_{2c}(r) \cos 2\phi + I_{2s}(r) \sin 2\phi$ , etc. (see the first equation in §§ 3.1).

Figure 21 displays a concrete example; it shows the reduced and deprojected SDSS i-band image of KIG 281 and the reconstructed  $m = 1, 2, 3, 4, 5$  Fourier term images. KIG 281 has two symmetric spiral arms ( $\cos 2\phi$  periodicity), therefore the dominant Fourier term is  $m=2$ . From a practical point of view, the Fourier terms with a nontrivial contribution to the spiral structure of a galaxy are those that match visually observable features in the deprojected image. In all cases the spiral structure is fully reconstructed without including terms beyond  $m=6$  and in most cases the first three terms suffice.

In this subsection we consider for analysis only 86 galaxies. Seven out of 93 galaxies do not show clear spiral arm morphology in their images. Therefore, we exclude them from the analysis of the  $m = 1-6$  Fourier term images performed in this subsection. Table 8 offers a census of spiral arm multiplicity encountered among the  $N=86$  sample of isolated galaxies that are subject to Fourier analysis.

About 40% of the galaxies in our sample ( $N=86$ ) have **only** a two-armed pattern ( $m=2$ ),  $\sim 4\%$  have **only** a three-armed pattern ( $m=3$ ) and  $\sim 1\%$  have **single**  $m=1$  spiral arms.

About 87% of our galaxies harbor  $m=2$  spiral arms,  $\sim 38\%$  have  $m=3$  spiral arms and  $\sim 20\%$  host  $m=1$  spiral arms. 13% of the galaxies have both  $m=1$  and  $m=2$  spiral arms. About 28% of the galaxies in our sample have both  $m=2$  and  $m=3$  spiral arms, with the two-armed pattern usually in the inner part of the galaxy and  $m=3$  spiral arms in the outer part. A representative example in this sense would be KIG 260. Figure 22 displays the SDSS i-band image of KIG 260 and the  $m=1, 2, 3$  Fourier terms images. One could easily notice two inner spiral arms ( $m=2$ ) starting at the end of the bar and three spiral arms ( $m=3$ ) in the outer part of the galaxy.

A particularly intriguing case is galaxy KIG 652. It was classified as SAB in our previous paper (Durbala et al. 2008). The best bulge-disk-bar decomposition solution returned by the BUDDA included a bar component for this galaxy. The reconstruction of the  $m=1-6$  Fourier terms revealed that the bar is not real and in fact there are two counter-winding inner spiral arms that mimic a bar-like feature in an image that is not deprojected (as used by the BUDDA code). Figure 23 displays the reduced and deprojected SDSS i-band image and the  $m = 1, 2, 3$  Fourier images. In the  $m=2$  image one can see the two inner counter-winding spiral arms (very open). The  $m=3$  image shows the three outer spiral arms. KIG 652 has  $m=2$  and  $m=3$  spiral arms winding in opposite directions. The  $m = 3$  Fourier images of KIG 260 and KIG 652 (Figures 22 and 23, respectively) show possible counterwinding spiral structure in their inner regions. However, within resolution and deepness constraints we cannot confirm those structures by direct visual inspection of the deprojected SDSS i-band images.

Another interesting case is KIG 282, whose deprojected SDSS image is shown in Figure 24 along with the Fourier reconstructed images corresponding to  $m=1$  through 3 terms. KIG 282 is a barred galaxy that displays both  $m=2$  and  $m=3$  spiral arm morphology. It is rather rare to see that a spiral arm in the  $m=3$  image originates very close to the bulge making a  $\sim 45^\circ$  angle with the bar. The other

two arms of the  $m=3$  term show a smooth continuity with the  $m=2$  arms, which appear joined to the end regions of the bar.

## 5 DISCUSSION

We have reported here the results of a Fourier decomposition analysis for a representative sample of Sb-Sc isolated (CIG/AMIGA) galaxies. This complements our earlier surface photometric analysis (Durbala et al. 2008) for the same sample. Our primary goal has been to characterize the structural properties of galaxies likely to have been least affected by external stimuli. The most common (2/3) kind of isolated galaxy appears to be the late-type spiral (Sb-Sc). This minimal-nurture sample can provide important clues about the formation, evolution and interplay of galactic components without the confusion added by external influences. We have focused here on measures involving the bar and spiral arm components. We now consider the main results of this paper in the light of some theoretical predictions and by comparing them to other samples of disk galaxies selected without isolation criteria.

### 5.1 Properties of Bars

Our Fourier analysis reveals that about 50% of our sample are barred spirals. We tested whether the barred and non-barred subsamples are different in terms of isolation (isolation parameters, i.e., tidal strengths for AMIGA galaxies were quantified in Verley et al. 2007a), absolute magnitude  $M_i$ , size  $a_{25}^i$  and color ( $g-i$ ) (tabulated in Durbala et al. 2008). We find no statistical difference between barred and non-barred galaxies in terms of isolation measures. This is in agreement with the recent study of Li et al. (2009), where they report no clustering differences between barred and non-barred galaxies based on a large sample of  $n=675$  SDSS spiral galaxies. The barred and nonbarred galaxies in our sample are very similar in absolute magnitude and size, the only statistically significant difference is found for the color ( $g-i$ ), median colors are 0.88 and 0.72 for barred and unbarred, respectively. This is probably expected given the observed tendency of stellar bars to show higher contrast in red and near-IR filters (see section 3.1 of Kormendy & Kennicutt 2004 and references therein). And this is also tied to the fact that the color gets bluer from Sb to Sc, the earlier bin (Sb) having the largest fraction of barred galaxies (Durbala et al. 2008).

Various studies attribute the term “strength” for different bar measures, e.g. Athanassoula (2003) refers as “strength” to a measure  $S_B$  more similar to our “contrast” terms  $A_{mb}$ , defined in § 4. Simulation studies (e.g. Athanassoula & Misiriotis 2002; Athanassoula 2003) predict an anticorrelation between  $S_B$  and the bar pattern speed. Sellwood (2000) suggested that within a disk galaxy the spiral component can transfer material to the bar, thus making it longer and reducing its pattern speed. This is also suggested by more recent simulations (e.g. Martinez-Valpuesta, Shlosman & Heller 2006). From these two major theoretical conclusions it could be inferred that the longer a bar becomes, the larger  $A_{mb}$  gets. Our results do confirm such theoretical predictions. We find that although the longer bars are not necessarily stronger (in terms of our  $Q_b$  torque) than the shorter ones (Figure 18a), the longer bars show higher contrast, i.e. there is a positive correlation between  $A_{2b}$  (maximum Fourier relative amplitudes in  $m=2$ ) and Fourier bar length  $l_{bar}$  (Figures 18b,c). This is also seen in the OSU sample (Figure 20). The fact that our observed correlations in Figures 18b,c are not very strong (correlation

coefficients  $\sim 0.7$ ) is in very good agreement with the numerical simulations that show a wide possible range of exchanged angular momentum between galactic components (Athanasoula 2003).

The role of gas in the process of bar formation, growth and interaction with the other major galactic components is still being debated (e.g. Berentzen et al. 2007). By transferring angular momentum a bar can contribute to the build-up of central mass concentrations, which in turn could lead to a declining bar (Pfenniger & Norman 1990; Norman, Sellwood & Hasan 1996), but probably not to the extent of complete destruction (Shen & Sellwood 2004; Athanasoula, Lambert & Dehnen 2005; Bournaud, Combes & Semelin 2005). The interpretation of observational results is further complicated by considering the role of the so-called “buckling instability” (e.g. Debattista et al. 2006; Martinez-Valpuesta, Shlosman & Heller 2006), which could weaken the bar within 2-3 Gyr of its formation.

Moreover, bars in gas rich spiral galaxies might be short lived structures and in typical Sb-Sc galaxies a bar can practically dissolve in 2 Gyr (Bournaud & Combes 2002). This is smaller than the time scale over which our isolated galaxies have not been visited by a similar size neighbor,  $\sim 3$  Gyr (Verdes-Montenegro et al. 2005). The presence of gas in galactic disks is responsible for both the destruction and renewal of bars when the gas is accreted from outside the disk (Bournaud & Combes 2002; Block et al. 2002). Simulations with sufficient resolution allow one to see the cyclic process of formation, destruction and reformation of bars (Heller, Shlosman & Athanasoula 2007).

According to Block et al. (2002) the fate of pure isolated disks (i.e. closed systems that do not accrete mass from outside) is that they “would become unbarred and their spiral structure would disappear; many disks would then be nearly axisymmetric after a few Gyr”. Block et al. (2002) argue that the observed strength (torque) distribution for disk galaxies with a striking depression at low values and an extended tail at large values<sup>6</sup> can be accounted for only by considering that spiral galaxies are open systems, actively and *continuously* accreting mass today (see also Sellwood & Carlberg 1984). The origin of the accreted gas is not considered, but it appears that accretion of dwarf satellites is far from enough in their simulations. The CIG/AMIGA isolated galaxies also lack large companions by definition. In the light of such arguments, one can conclude that the accreted matter must come from either some sort of galactic internal reservoirs or from intergalactic cosmic filaments (Combes 2008). A very recent study (Bekki, Tsujimoto & Chiba 2009) investigates, using numerical simulations, “whether and how stellar winds from bulges (or stellar ejecta due to supernova feedback) can be accreted onto the disks after hydrodynamical interaction with the gaseous halos”. Although that study explores a chemical connection between bulge and disk components, it certainly proposes a viable mechanism to add new mass onto the disks.

The fate of bars can be significantly affected by tidal interactions (e.g. Noguchi 1987; Gerin, Combes & Athanasoula 1990; Miwa & Noguchi 1998; Berentzen et al. 2003, 2004). We consider that CIG/AMIGA are minimally affected by external interactions. We looked for trends/correlations between tidal strengths (Verley et al. 2007a) and estimated bar, spiral and total torque strength parameters for the galaxies in our sample and found none. We should also point out that no correlation was found between the basic structural parameters of the bulge, disk and bar presented in

Durbala et al. (2008) and the tidal strength measures quantified in Verley et al. (2007a).

We find that  $Q_b$  and  $l_{bar}$  do not correlate for our CIG/AMIGA sample. We also explore this torque-bar length relation by comparing our isolated galaxies with the OSU sample (Tables 3 and 6). Even though the CIG/AMIGA galaxies host longer bars<sup>7</sup> (the difference being most noticeable for Sb and Sbc types) we do not find stronger  $Q_b$  measures for the CIG/AMIGA isolated galaxies.

The observed low occurrence of strong bars in both CIG/AMIGA and OSU (see Figures 12 and 19b) may indicate either that strong bars are very transient and/or they are allowed only by special conditions (Buta et al. 2005), apparently not sampled by either of the two samples.

## 5.2 Bar-Spiral Connection

We find that in  $\sim 74\%$  of the barred galaxies the strength of bars dominates over the spiral arm strength (Table 1). This is also seen in Table 3 where within each morphological bin  $Q_b > Q_s$  in isolated galaxies and in Table 6 for the OSU sample. We find that in our sample  $Q_g$  is a very reliable tracer of the bar strength  $Q_b$  (Figure 16a).

A very recent study (Buta et al. 2009) has examined on empirical grounds the connection between the torque strength of bars and spiral structure using near-IR  $K_s$ -band images for 23 galaxies that are morphologically diverse. They find weak but definite indications that stronger spirals are associated with stronger bars (see also Block et al. 2004); their correlation is relevant for  $Q_b > 0.3$ . Perhaps the energy and angular momentum exchange due to resonance coupling between bar and spiral components (Tagger et al. 1987; Sygnet et al. 1988) is reflected in a  $Q_b - Q_s$  correlation only for this restricted  $Q_b > 0.3$  regime.

Our data do not show any trend or correlation between the two measures  $Q_b$  and  $Q_s$  (Figure 15(a)). However, our sample includes only 13 (out of 46 barred) galaxies with strong  $Q_b > 0.3$  measures. From this point of view, in the isolated galaxies investigated here bars and spirals appear to be more independent features (see also Sellwood & Sparke 1988).

## 5.3 Properties of Spiral Arms

It is worth noting that in Figure 15(b), where we plot spiral strength  $Q_s$  versus bar contrast  $A_{2b}$ , we see a clear morphological separation, although no correlation is observed in this plot either. We find that bar strength and bar contrast (Figure 13 (a)-(c)) are very well correlated in Sbc-Sc types (see section §§ 4.3), but the Sb galaxies depart from that correlation along the abscissa and they spread over a larger bar contrast range. It is also worth indicating that on average the Sb galaxies show the largest differences in almost all Fourier measures when comparing isolated and OSU galaxies.

Fourier decomposition can reveal surprising cases of counter-winding spiral structure (KIG 652 / NGC 5768). Only a few other similar cases are known in literature: NGC 4622 (Buta, Byrd & Freeman 2003), ESO 297-27 (Grouchy et al. 2008), NGC 3124 (Purcell 1998; Buta 1999) and IRAS 18293-3413 (Väisänen et al. 2008).

<sup>6</sup> Note that Block et al. (2002) employ the OSU sample using a constant radial to vertical  $h_r/h_z = 12$  ratio for all morphological types.

<sup>7</sup> The isolated galaxies show larger bars than OSU galaxies both in terms of Fourier bars analyzed herein on deprojected images and also in terms of bar size derived from 2D light decomposition of projected images (Durbala et al. 2008).



We would like at this point to evaluate the relative frequency of certain spiral arm multiplicities in our sample of isolated Sb-Sc galaxies in contrast to other similar studies. The only reference where a study of spiral arm multiplicity is available is the Catalog of Southern Ringed Galaxies (CSRG; Buta 1995). However, one should keep in mind that the CSRG galaxies were evaluated in terms of such multiplicities by direct visual inspection of their images, without any Fourier analysis or prior deprojection of images. CSRG is a special catalog in itself being a collection of “ringed” galaxies. This is why we caution the reader that any inference we make in the light of the comparison of our sample against CSRG could be seen as speculative for the time being. Using the on-line access to CSRG through Vizier<sup>8</sup> we extracted from CSRG only the Sb-Sc galaxies, i.e. morphological types T=3-5. We considered both the full sample thus obtained, but also a more “restricted” subset imposing the conditions explained in Buta (1995) (relative to his Table 8). This latter subset is also considered more reliable for statistical purposes.

Two-armed spiral patterns are the most frequent among isolated Sb-Sc galaxies ( $\sim 40\%$ ). Among the Sb-Sc of the CSRG the fraction of  $m = 2$  is 31-33 % and still the most frequent mode. However, large differences are noted for  $m = 2$  & 3 spiral arm multiplicity. We find in our sample 24 out of 86  $m = 2$  & 3 galaxies (28%). The CSRG-based comparison sample includes 6-8% such cases. However, we note that the definitions employed by Buta (1995) are not the same ones applied herein (i.e. what we call here 2 & 3 would most likely be equivalent to 1+2, 2+1 and 3 altogether in that reference). We cannot assess at this time whether the rarity of 2 & 3 multiplicity combination is due to the special nature of that CSRG catalog or it is a phenomenon more likely to occur in isolated galaxies. But it is particularly interesting to indicate here that the high rate of occurrence of  $m = 2$  & 3 combination among CIG/AMIGA galaxies may be linked to their isolation (Elmegreen, Elmegreen & Montenegro 1992). The formation of strong three-arm structures may require long episodes without strong tidal perturbations (“*Perhaps three-arm structures will provide a good measure of the time that has elapsed since a tidal interaction*” - Elmegreen, Elmegreen & Montenegro 1992). Moreover, the fact that the  $Q_s$  distribution for CIG/AMIGA is significantly different than that of OSU (§§ 4.7) may be tied to the isolation, too.

## 6 CONCLUSIONS

Our Fourier decomposition analysis applied to a representative sample of  $n \sim 100$  isolated CIG/AMIGA galaxies allows several important conclusions:

- both the length ( $l_{bar}$ ) and the contrast (e.g.  $A_{2b}$ ) of the Fourier bars decrease along the morphological sequence Sb-Sbc-Sc, with bars in earlier types being longer and showing higher contrast;
- a tight correlation between the bar strength  $Q_b$  and the bar contrast (e.g.  $A_{2b}$ ; Figure 13a) is evident for Sbc-Sc types, while Sb galaxies seem to depart from the trend, being clearly separated in bar contrast measures;
- longer bars are not necessarily stronger (as indicated by the torque measures), but longer bars show higher Fourier contrast (i.e. relative amplitudes), in very good agreement with theoretical predictions;
- bar and spiral galactic components are independent in the sense

that the dynamical torque-strengths of the two components are not correlated;

- the total strength  $Q_g$  is a very reliable tracer of the bar strength  $Q_b$ ;
- for the large majority of the barred galaxies in our sample ( $\sim 74\%$ ) the strength of the bar dominates over the spiral arm strength ( $Q_b > Q_s$ ), which is also noted in the OSU comparison sample;
- barred and non-barred galaxies show similar spiral arm strengths  $Q_s$ , while the total non-axisymmetric strength  $Q_g$  is about  $1.5 \times$  larger in barred relative to the non-barred galaxies (in each morphological bin Sb-Sbc-Sc);
- comparison with samples of galaxies of the same morphological types defined and selected without isolation criteria (e.g. OSU sample) indicates that the isolated CIG/AMIGA galaxies host longer Fourier bars and possibly have a different distribution of spiral torque strength  $Q_s$ ;
- Fourier decomposition can reveal surprisingly rare cases of counterwinding spiral structure (e.g. KIG 652/NGC 5768);
- our sample of isolated Sb-Sc galaxies is dominated by  $m=2$  spiral arm multiplicity ( $\sim 40\%$ );
- $m = 2$  & 3 spiral arm components appear present in  $\sim 28\%$  of our sample and this rather large rate of occurrence may indicate a long time without external tidal perturbations (Elmegreen, Elmegreen & Montenegro 1992).

## ACKNOWLEDGMENTS

AD and RB acknowledge support of NSF Grant AST 05-07140.

This study has made use of SDSS Data Release 6. Funding for the SDSS and SDSS-II has been provided by the Alfred P. Sloan Foundation, the Participating Institutions, the National Science Foundation, the U.S. Department of Energy, the National Aeronautics and Space Administration, the Japanese Monbukagakusho, the Max Planck Society, and the Higher Education Funding Council for England. The SDSS Web Site is <http://www.sdss.org/>. The SDSS is managed by the Astrophysical Research Consortium for the Participating Institutions. The Participating Institutions are the American Museum of Natural History, Astrophysical Institute Potsdam, University of Basel, University of Cambridge, Case Western Reserve University, University of Chicago, Drexel University, Fermilab, the Institute for Advanced Study, the Japan Participation Group, Johns Hopkins University, the Joint Institute for Nuclear Astrophysics, the Kavli Institute for Particle Astrophysics and Cosmology, the Korean Scientist Group, the Chinese Academy of Sciences (LAM-OST), Los Alamos National Laboratory, the Max-Planck-Institute for Astronomy (MPIA), the Max-Planck-Institute for Astrophysics (MPA), New Mexico State University, Ohio State University, University of Pittsburgh, University of Portsmouth, Princeton University, the United States Naval Observatory, and the University of Washington.

This research has made use of the Vizier catalogue access tool, CDS, Strasbourg, France.

The authors kindly thank the reviewer for many helpful comments and suggestions.

<sup>8</sup> <http://vizier.cfa.harvard.edu>

## REFERENCES

- Athanassoula, E. & Misiriotis, A. 2002, MNRAS, 330, 35
- Athanassoula, E. 2003, MNRAS, 341, 1179
- Athanassoula, E., Lambert, J. C. & Dehnen, W. 2005, MNRAS, 363, 496
- Bekki, K., Tsujimoto, T. & Chiba, M. 2009 - arXiv:0901.1355
- Berentzen, I., Athanassoula, E., Heller, C. H., Fricke, K. J. 2003, MNRAS, 341, 343
- Berentzen, I., Athanassoula, E., Heller, C. H., Fricke, K. J. 2004, MNRAS, 347, 220
- Berentzen, I., Shlosman, I. & Jogee, S. 2006, ApJ, 637, 582
- Berentzen, I., Shlosman, I., Martinez-Valpuesta, I., Heller, C. H. 2007, ApJ, 666, 189
- Block, D. L., Bournaud, F., Combes, F., Puerari, I., Buta, R. 2002, A&A, 394, L35
- Block, D. L., Buta, R., Knapen, J. H., Elmegreen, D. M., Elmegreen, B. G., Puerari, I. 2004, AJ, 128, 183
- Bournaud, F. & Combes, F. 2002, A&A, 392, 83
- Bournaud, F., Combes, F. & Semelin, B. 2005, MNRAS, 364, L18
- Buta, R. 1995, ApJS, 96, 39
- Buta, R. 1999, Ap&SS, 269, 79
- Buta, R. & Block, D. L. 2001, ApJ, 550, 243
- Buta, R., Block, D. L. & Knapen, J. H. 2003, AJ, 126, 1148
- Buta, R. J., Byrd, G. G. & Freeman, T. 2003, AJ, 125, 634
- Buta, R., Laurikainen, E. & Salo, H. 2004, AJ, 127, 279
- Buta, R., Vasylyev, S., Salo, H., Laurikainen, E. 2005, AJ, 130, 506
- Buta, R. J., Knapen, J. H., Elmegreen, B. G., Salo, H., Laurikainen, E., Elmegreen, D. M., Puerari, I., Block, D. L. 2009 - arXiv:0903.2008
- Li, C., Gadotti, D. A., Mao, S., Kauffmann, G. 2009 - arXiv:0902.1175
- Combes, F. & Sanders, R. H. 1981, A&A, 96, 164
- Combes, F. in "Formation and Evolution of Galaxy Bulges", Proceedings of the International Astronomical Union, 2008 IAU Symposium, Volume 245, p. 151-160
- Considera, S. & Athanassoula, E. 1988, A&AS, 76, 365
- Debattista, V. P., Mayer, L., Carollo, C. M., Moore, B., Wadsley, J., Quinn, T. 2006, ApJ, 645, 209
- de Grijs, R. 1998, MNRAS, 299, 595
- de Souza, R. E., Gadotti, D. A. & dos Anjos, S. 2004, ApJS, 153, 411
- de Vaucouleurs, G., de Vaucouleurs, A., Corwin, H. G., Jr., Buta, R. J., Paturel, G., Fouque, P. 1991, Third Reference Catalog of Bright Galaxies (New York: Springer) (RC3)
- Durbala, A., Sulentic, J. W., Buta, R., Verdes-Montenegro, L. 2008, MNRAS, 390, 881
- Elmegreen, B. G. & Elmegreen, D. M. 1989, ApJ, 342, 677
- Elmegreen, B. G., Elmegreen, D. M. & Montenegro, L. 1992, ApJS, 79, 37
- Elmegreen, B. G., Elmegreen, D. M., Knapen, J. H., Buta, R. J., Block, D. L., Puerari, I. 2007, ApJ, 670, L97
- Eskridge, P. B. et al. 2002, ApJS, 143, 73
- Gerin, M., Combes, F. & Athanassoula, E. 1990, A&A, 230, 37
- Grouchy, R. D., Buta, R., Salo, H., Laurikainen, E., Speltinckx, T. 2008, AJ, 136, 980
- Heller, C. H., Shlosman, I. & Athanassoula, E. 2007, ApJ, 657, L65
- Karachentseva, V. E. 1973 *Astrofizicheskie Issledovaniia Izvestiya Spetsialnoj Astrofizicheskoy Observatorii*, 8, 3
- Kormendy, J. & Kennicutt, R. C., Jr. 2004, ARAA, 42, 603
- Laurikainen, E. & Salo, H. 2002, MNRAS, 337, 1118
- Laurikainen, E., Salo, H., Buta, R., Vasylyev, S. 2004, MNRAS, 355, 1251
- Laurikainen, E., Salo, H. & Buta, R. 2005, MNRAS, 362, 1319
- Martinez-Valpuesta, I., Shlosman, I. & Heller, C. 2006, ApJ, 637, 214
- Miwa, T. & Noguchi, M. 1998, ApJ, 499, 149
- Noguchi, M. 1987, MNRAS, 228, 635
- Noguchi, M. 1996, ApJ, 469, 605
- Noguchi, M. 2000, MNRAS, 312, 194
- Norman, C. A., Sellwood, J. A. & Hasan, H. 1996, ApJ, 462, 114
- Pfenniger, D. & Norman, C. 1990, ApJ, 363, 391
- Puerari, I. & Dottori, H. A. 1992, A&AS, 93, 469
- Purcell, G. B. 1998, Ph.D. Thesis, University of Alabama,
- Sanders, R. H. & Tubbs, A. D. 1980, ApJ, 235, 803
- Sellwood, J. A. & Carlberg, R. G. 1984, ApJ, 282, 61
- Sellwood, J. A. & Sparke, L. S. 1988, MNRAS, 231P, 25
- Sellwood, J. A. in "Dynamics of Galaxies: from the Early Universe to the Present", 15th IAP meeting held in Paris, France, July 9-13, 1999, Eds.: Françoise Combes, Gary A. Mamon, and Vassilis Charmandaris ASP Conference Series, Vol. 197, ISBN: 1-58381-024-2, 2000, p. 3.
- Shen, J. & Sellwood, J. A. 2004, ApJ, 604, 614
- Stoughton, C. et al. 2002, AJ, 123, 485
- Sulentic, J. W. et al. 2006, A&A, 449, 937
- Syget, J. F., Tagger, M., Athanassoula, E., Pellat, R. 1988, MNRAS, 232, 733
- Tagger, M., Syget, J. F., Athanassoula, E., Pellat, R. 1987, ApJ, 318, L43
- Väisänen, P., Ryder, S., Mattila, S., Kotilainen, J. 2008, ApJ, 689, L37
- Verdes-Montenegro, L., Sulentic, J., Lisenfeld, U., Leon, S., Espada, D., Garcia, E., Sabater, J., Verley, S. 2005, A&A, 436, 443
- Verley, S. et al. 2007a, A&A, 472, 121
- Verley, S., Combes, F., Verdes-Montenegro, L., Bergond, G., Leon, S. 2007b, A&A, 474, 43

**Table 1.** Fourier-derived Parameters in i-band for the CIG/KIG Galaxies in our Sample

(1) Galaxy Name	(2) orientation angle ( $^{\circ}$ )	(3) bulge method	(4) $Q_g$	(5) $Q_b$	(6) $Q_s$	(7) $A_{2b}$	(8) $A_{4b}$	(9) $A_{6b}$	(10) $l_{bar}$ (arcsec)	(11) $r(Q_b)$ (arcsec)
KIG 011	77	a	$0.091 \pm 0.040$		$0.091 \pm 0.040$					
KIG 033	178	c	$0.183 \pm 0.082$		$0.183 \pm 0.082$					
KIG 056	71	a	$0.293 \pm 0.023$	$0.227 \pm 0.023$	$0.166 \pm 0.022$	0.529	0.255	0.151	19.0	11.0
KIG 187	99	a	$0.134 \pm 0.008$	$0.080 \pm 0.002$	$0.126 \pm 0.080$	0.175	0.053		8.0	5.5
KIG 198	72	a	$0.176 \pm 0.020$	$0.108 \pm 0.001$	$0.171 \pm 0.015$	0.217			12.0	7.0
KIG 203	173	b	$0.136 \pm 0.052$		$0.136 \pm 0.052$					
KIG 217	172	a	$0.183 \pm 0.010$		$0.183 \pm 0.010$					
KIG 222	46	a	$0.236 \pm 0.055$	$0.184 \pm 0.055$	$0.165 \pm 0.003$	0.282	0.092	0.043	11.0	8.0
KIG 232	46	a	$0.391 \pm 0.094$		$0.391 \pm 0.094$					
KIG 238	178	a	$0.358 \pm 0.074$	$0.286 \pm 0.004$	$0.235 \pm 0.089$	0.697	0.405	0.202	12.0	8.0
KIG 241	178	a	$0.260 \pm 0.080$		$0.260 \pm 0.080$					
KIG 242	102	a	$0.150 \pm 0.032$		$0.150 \pm 0.032$					
KIG 258	34	b	$0.214 \pm 0.042$	$0.205 \pm 0.024$	$0.115 \pm 0.038$	0.439	0.125	0.071	9.0	8.0
KIG 260	124	a	$0.190 \pm 0.038$	$0.156 \pm 0.011$	$0.178 \pm 0.062$	0.155	0.034		8.0	4.0
KIG 271	159	c	$0.156 \pm 0.047$		$0.156 \pm 0.047$					
KIG 281	130	a	$0.095 \pm 0.011$		$0.095 \pm 0.011$					
KIG 282	135	a	$0.234 \pm 0.022$	$0.230 \pm 0.015$	$0.175 \pm 0.050$	0.277	0.053	0.024	8.5	4.0
KIG 287	61	c	$0.230 \pm 0.027$	$0.220 \pm 0.019$	$0.114 \pm 0.021$	0.364	0.117	0.058	15.0	7.0
KIG 292	39	a	$0.307 \pm 0.065$		$0.307 \pm 0.065$					
KIG 298	110	a	$0.202 \pm 0.031$	$0.167 \pm 0.013$	$0.127 \pm 0.016$	0.417	0.200	0.103	14.0	10.5
KIG 302	5	a	$0.443 \pm 0.078$		$0.443 \pm 0.078$					
KIG 314	110	a	$0.137 \pm 0.045$		$0.137 \pm 0.045$					
KIG 325	53	a	$0.151 \pm 0.061$		$0.151 \pm 0.061$					
KIG 328	14	c	$0.170 \pm 0.021$		$0.170 \pm 0.021$					
KIG 330	173	a	$0.172 \pm 0.089$		$0.172 \pm 0.089$					
KIG 336	54	a	$0.332 \pm 0.043$	$0.330 \pm 0.026$	$0.059 \pm 0.005$	0.564	0.333	0.230	25.0	16.5
KIG 339	167	a	$0.180 \pm 0.008$	$0.175 \pm 0.012$	$0.092 \pm 0.045$	0.833	0.357	0.193	19.0	12.0
KIG 351	121	a	$0.509 \pm 0.043$	$0.504 \pm 0.018$	$0.079 \pm 0.038$	0.616	0.289	0.166	11.0	8.0
KIG 365	99	a	$0.314 \pm 0.033$	$0.269 \pm 0.018$	$0.203 \pm 0.069$	0.292	0.106	0.050	8.5	5.0
KIG 366	113	a	$0.338 \pm 0.052$	$0.311 \pm 0.051$	$0.168 \pm 0.063$	0.560	0.220	0.100	19.0	11.0
KIG 367	81	a	$0.139 \pm 0.053$		$0.139 \pm 0.053$					
KIG 368	47	a	$0.220 \pm 0.053$		$0.220 \pm 0.053$					
KIG 386	136	a	$0.181 \pm 0.050$	$0.137 \pm 0.027$	$0.164 \pm 0.057$	0.209	0.069	0.028	5.5	4.0
KIG 397	148	b	$0.207 \pm 0.077$		$0.207 \pm 0.077$					
KIG 399	14	a	$0.199 \pm 0.024$		$0.199 \pm 0.024$					
KIG 401	132	c	$0.286 \pm 0.019$		$0.286 \pm 0.019$					
KIG 405	101	a	$0.199 \pm 0.084$	$0.094 \pm 0.015$	$0.200 \pm 0.084$	0.134			3.0	1.0
KIG 406	32	a	$0.156 \pm 0.055$		$0.156 \pm 0.055$					
KIG 409	122	a	$0.291 \pm 0.061$	$0.210 \pm 0.014$	$0.293 \pm 0.056$	0.201	0.045		4.0	2.0
KIG 410	5	a	$0.238 \pm 0.128$		$0.238 \pm 0.128$					
KIG 429	124	a	$0.183 \pm 0.064$		$0.183 \pm 0.064$					
KIG 444	25	a	$0.268 \pm 0.078$	$0.180 \pm 0.002$	$0.266 \pm 0.078$	0.171			2.5	2.0
KIG 446	154	b	$0.091 \pm 0.031$		$0.091 \pm 0.031$					
KIG 460	168	c	$0.170 \pm 0.027$	$0.169 \pm 0.010$	$0.122 \pm 0.010$	0.142	0.061	0.044	5.5	3.0
KIG 466	52	a	$0.396 \pm 0.054$	$0.388 \pm 0.011$	$0.134 \pm 0.042$	0.277	0.100	0.042	11.8	1.0
KIG 489	178	a	$0.249 \pm 0.100$		$0.249 \pm 0.100$					
KIG 491	39	a	$0.074 \pm 0.010$		$0.074 \pm 0.010$					
KIG 494	77	a	$0.277 \pm 0.136$	$0.241 \pm 0.017$	$0.241 \pm 0.082$	0.220	0.032		4.0	1.0
KIG 499	72	b	$0.261 \pm 0.033$	$0.239 \pm 0.011$	$0.140 \pm 0.043$	0.539	0.217	0.090	10.2	7.0
KIG 502	15	b	$0.119 \pm 0.019$		$0.119 \pm 0.019$					
KIG 508	80	a	$0.404 \pm 0.088$	$0.370 \pm 0.005$	$0.254 \pm 0.119$	0.555	0.222	0.051	6.0	2.0
KIG 512	136	a	$0.382 \pm 0.068$	$0.368 \pm 0.016$	$0.187 \pm 0.037$	0.364	0.140	0.052	17.0	3.0
KIG 515	140	a	$0.161 \pm 0.037$	$0.108 \pm 0.004$	$0.161 \pm 0.037$	0.076			4.5	1.0
KIG 520	85	a	$0.075 \pm 0.014$	$0.058 \pm 0.020$	$0.075 \pm 0.014$	0.100			3.5	2.0
KIG 522	107	a	$0.306 \pm 0.021$	$0.205 \pm 0.019$	$0.188 \pm 0.038$	0.357	0.116	0.038	5.0	3.0
KIG 525	34	a	$0.231 \pm 0.022$	$0.199 \pm 0.001$	$0.189 \pm 0.037$	0.389	0.233	0.128	12.2	9.0
KIG 532	16	a	$0.492 \pm 0.148$	$0.490 \pm 0.013$	$0.222 \pm 0.081$	0.528	0.185	0.074	6.0	2.0
KIG 550	57	a	$0.244 \pm 0.025$	$0.223 \pm 0.001$	$0.143 \pm 0.037$	0.432	0.214	0.123	15.0	10.0
KIG 553	50	a	$0.192 \pm 0.010$	$0.132 \pm 0.011$	$0.140 \pm 0.009$	0.562	0.300	0.206	20.0	11.0
KIG 560	161	a	$0.252 \pm 0.024$	$0.230 \pm 0.012$	$0.184 \pm 0.058$	0.238	0.044		4.5	1.0
KIG 571	125	b	$0.103 \pm 0.028$		$0.103 \pm 0.028$					
KIG 575	52	a	$0.080 \pm 0.036$		$0.080 \pm 0.036$					

**Table 1.**–continued

(1) Galaxy Name	(2) orientation angle (°)	(3) bulge method	(4) $Q_g$	(5) $Q_b$	(6) $Q_s$	(7) $A_{2b}$	(8) $A_{4b}$	(9) $A_{6b}$	(10) $l_{bar}$ (arcsec)	(11) $r(Q_b)$ (arcsec)
KIG 580	132	a	$0.149 \pm 0.054$		$0.149 \pm 0.054$					
KIG 598	62	c	$0.250 \pm 0.043$		$0.250 \pm 0.043$					
KIG 612	103	a	$0.205 \pm 0.014$	$0.189 \pm 0.001$	$0.091 \pm 0.018$	0.473	0.244	0.108	10.8	7.0
KIG 626	155	a	$0.292 \pm 0.142$	$0.279 \pm 0.011$	$0.288 \pm 0.060$	0.225	0.057		10.0	3.0
KIG 630	64	a	$0.175 \pm 0.062$		$0.175 \pm 0.062$					
KIG 633	70	a	$0.113 \pm 0.069$		$0.113 \pm 0.069$					
KIG 639	20	b	$0.139 \pm 0.034$		$0.139 \pm 0.034$					
KIG 640	30	a	$0.084 \pm 0.036$		$0.084 \pm 0.036$					
KIG 641	45	a	$0.225 \pm 0.018$	$0.197 \pm 0.003$	$0.113 \pm 0.034$	0.409	0.178	0.107	12.0	9.0
KIG 645	0	b	$0.145 \pm 0.036$		$0.145 \pm 0.036$					
KIG 652	120	a	$0.217 \pm 0.068$		$0.217 \pm 0.068$					
KIG 665	70	a	$0.093 \pm 0.048$		$0.093 \pm 0.048$					
KIG 671	117	c	$0.362 \pm 0.052$	$0.336 \pm 0.003$	$0.161 \pm 0.100$	1.003	0.561	0.349	16.5	10.5
KIG 689	80	a	$0.280 \pm 0.144$	$0.240 \pm 0.006$	$0.137 \pm 0.095$	0.200	0.045		6.0	1.0
KIG 712	152	b	$0.412 \pm 0.093$	$0.365 \pm 0.026$	$0.161 \pm 0.050$	0.504	0.243	0.147	33.0	18.0
KIG 716	122	b	$0.090 \pm 0.031$		$0.090 \pm 0.031$					
KIG 719	98	b	$0.450 \pm 0.042$	$0.423 \pm 0.005$	$0.209 \pm 0.063$	0.673	0.403	0.237	13.8	10.5
KIG 731	108	a	$0.384 \pm 0.077$	$0.380 \pm 0.030$	$0.101 \pm 0.025$	0.417	0.237	0.103	7.0	5.0
KIG 743	24	c	$0.385 \pm 0.040$	$0.380 \pm 0.066$	$0.067 \pm 0.017$	0.515	0.220	0.106	13.0	11.0
KIG 757	39	c	$0.152 \pm 0.030$		$0.152 \pm 0.030$					
KIG 795	92	b	$0.339 \pm 0.088$	$0.333 \pm 0.018$	$0.292 \pm 0.058$	0.400	0.091	0.068	11.0	6.0
KIG 805	35	b	$0.113 \pm 0.015$		$0.113 \pm 0.015$					
KIG 807	25	a	$0.161 \pm 0.074$		$0.161 \pm 0.074$					
KIG 839	164	b	$0.197 \pm 0.059$		$0.197 \pm 0.059$					
KIG 892	122	a	$0.208 \pm 0.084$		$0.208 \pm 0.084$					
KIG 912	91	b	$0.117 \pm 0.047$		$0.117 \pm 0.047$					
KIG 924	165	a	$0.093 \pm 0.018$		$0.093 \pm 0.018$					
KIG 928	153	a	$0.061 \pm 0.038$		$0.061 \pm 0.038$					
KIG 931	111	a	$0.284 \pm 0.056$	$0.200 \pm 0.005$	$0.246 \pm 0.053$	0.301			5.5	2.0
KIG 932	5	c	$0.199 \pm 0.047$	$0.188 \pm 0.022$	$0.073 \pm 0.019$	0.326	0.109	0.046	12.2	8.0
KIG 943	178	b	$0.278 \pm 0.039$	$0.166 \pm 0.014$	$0.213 \pm 0.044$	0.614	0.272	0.122	8.0	5.0

Column (1): KIG Name. Column (2): mean orientation angle (measured as explained in §§§ 3.1.1). Column (3): bulge deprojection method used (see §§§ 3.1.1 for more details). Column (4): total strength  $Q_g \pm$  SD (standard deviation). Column (5): bar strength  $Q_b \pm$  SD. Column (6): spiral strength  $Q_s \pm$  SD. Column (7):  $A_{2b}$ . Column (8):  $A_{4b}$ . Column (9):  $A_{6b}$ . Column (10): Fourier bar length in arcsec. Column (11): radius of maximal bar torque  $r(Q_b)$  in arcsec.

**Table 2.** Mean/Median for Strength Parameters of **All** Galaxies in our sample

Type (N)	$Q_s$		$Q_g$	
	mean±SE	median	mean±SE	median
Sb (25)	0.151±0.012	0.161	0.285±0.019	0.278
Sbc (33)	0.157±0.012	0.151	0.178±0.014	0.170
Sc (35)	0.188±0.013	0.171	0.221±0.018	0.183
Sb-Sc (93)	0.167±0.007	0.161	0.223±0.012	0.202

Column (1): galaxy name. Column (2): spiral arm strength. Column (3): total strength.

Note: N=number of galaxies; SE is standard deviation of the mean.

**Table 3.** Mean/Median for Strength Parameters of **Barred** Galaxies in our sample

Type (N)	$Q_b$		$Q_s$		$Q_g$		$A_{2b}$		$l_{bar}$ (kpc)	
	mean±SE	median	mean±SE	median	mean±SE	median	mean±SE	median	mean±SE	median
Sb (22)	0.261±0.022	0.225	0.146±0.011	0.152	0.298±0.019	0.286	0.51±0.03	0.51	6.41±0.60	6.02
Sbc (10)	0.206±0.031	0.205	0.164±0.026	0.124	0.232±0.030	0.232	0.32±0.07	0.29	4.44±0.86	4.36
Sc (14)	0.242±0.033	0.235	0.199±0.013	0.186	0.282±0.027	0.273	0.25±0.04	0.22	2.32±0.43	2.01
Sb-Sc (46)	0.243±0.015	0.222	0.166±0.009	0.165	0.279±0.014	0.273	0.39±0.03	0.38	4.74±0.44	4.36

Column (1): galaxy name. Column (2): bar strength. Column (3): spiral arm strength. Column (4): total strength. Column (5):  $A_{2b} = (I_2/I_0)_{max}$ . Column (6) length of the bar in kpc.

Note: N=number of galaxies; SE is standard deviation of the mean.

**Table 4.** Mean/Median for Strength Parameters of **Non-Barred** Galaxies in our sample

Type (N)	$Q_s = Q_g$	
	mean±SE	median
Sb (3)	0.192±0.062	0.175
Sbc (23)	0.155±0.013	0.152
Sc (21)	0.181±0.020	0.149
Sb-Sc (47)	0.169±0.011	0.152

Column (1): galaxy name. Column (2): spiral arm strength = total strength.

Note: N=number of galaxies; SE is standard deviation of the mean. For non-barred galaxies  $Q_b \approx 0$ , therefore  $Q_g \simeq Q_s$ .

**Table 5.** Mean/Median for Strength Parameters of **All** Galaxies in the OSU sample

Type (N)	$Q_s$		$Q_g$	
	mean±SE	median	mean±SE	median
Sb (25)	0.113±0.018	0.097	0.205±0.025	0.197
Sbc (32)	0.187±0.022	0.157	0.256±0.026	0.254
Sc (35)	0.156±0.011	0.145	0.253±0.027	0.202
Sb-Sc (92)	0.155±0.010	0.132	0.241±0.015	0.210

Column (1): galaxy name. Column (2): spiral arm strength.  
Column (3): total strength.

Note: N=number of galaxies; *SE* is standard deviation of the mean.

**Table 6.** Mean/Median for Strength Parameters of **Barred** Galaxies in the OSU sample

Type (N)	$Q_b$		$Q_s$		$Q_g$		$A_{2b}$		$l_{bar}$ (kpc)	
	mean±SE	median	mean±SE	median	mean±SE	median	mean±SE	median	mean±SE	median
Sb (20)	0.204±0.023	0.196	0.111±0.014	0.099	0.227±0.023	0.227	0.48±0.04	0.45	4.33±0.78	3.13
Sbc (19)	0.240±0.033	0.225	0.194±0.030	0.169	0.310±0.034	0.259	0.50±0.05	0.42	3.72±0.60	3.04
Sc (21)	0.290±0.038	0.321	0.165±0.015	0.167	0.318±0.038	0.360	0.39±0.04	0.35	2.42±0.40	1.89
Sb-Sc (60)	0.246±0.019	0.212	0.156±0.013	0.137	0.285±0.019	0.254	0.45±0.03	0.41	3.47±0.36	2.64

Column (1): galaxy name. Column (2): bar strength. Column (3): spiral arm strength. Column (4): total strength. Column (5):  $A_{2b} = (I_2/I_0)_{max}$ . Column (6) length of the bar in kpc.

Note: N=number of galaxies; *SE* is standard deviation of the mean.

**Table 7.** Mean/Median for Strength Parameters of **Non-Barred** Galaxies in the OSU sample

Type (N)	$Q_g$	
	mean±SE	median
Sb (5)	0.117±0.075	0.039
Sbc (13)	0.176±0.031	0.148
Sc (14)	0.155±0.015	0.148
Sb-Sc (32)	0.158±0.018	0.143

Column (1): galaxy name. Column (2): total strength.

Note: N=number of galaxies; *SE* is standard deviation of the mean.

**Table 8.** Spiral Arm Multiplicities for a Selected Number of Galaxies in our Sample (N=86)

Multiplicity m	Number of galaxies N
1 .....	1
2 .....	34
3 .....	3
4 .....	2
1 & 2 .....	11
1 & 3 .....	2
1 & 4 .....	2
2 & 3 .....	24
2 & 4 .....	2
3 & 4 .....	1
1, 2 & 3 .....	2
1, 2 & 4 .....	1
2, 3 & 4 .....	1

Column (1): Spiral Arm multiplicities present in our sample. Column (2): Number of galaxies in each spiral arm multiplicity bin.

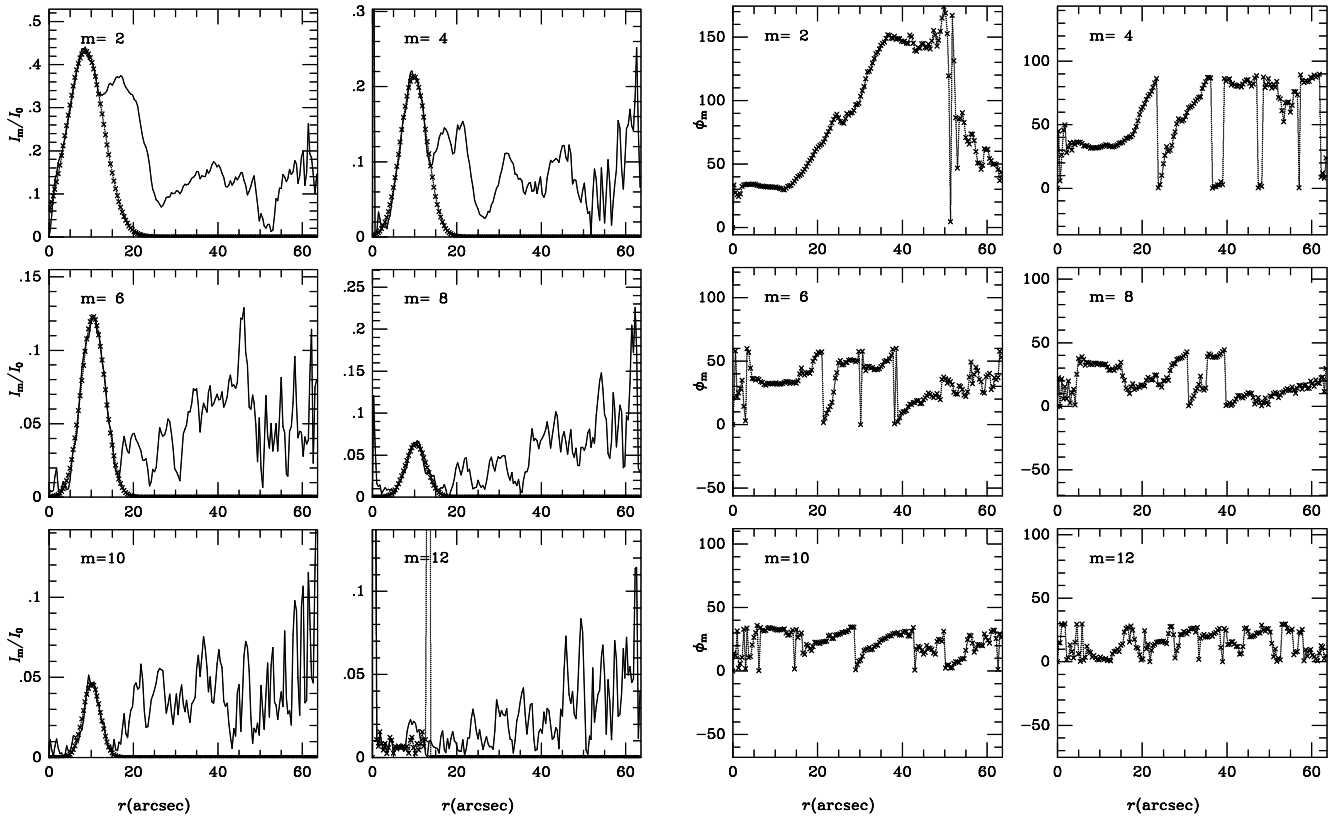


**Figure 1.** KIG 550: (*left*): Relative Fourier intensity amplitudes  $I_m/I_0$  for the first six even Fourier terms ( $m=2$  to  $m=12$ ); (*right*): Phase profiles  $\phi_m$  for the first six even Fourier terms ( $m=2$  to  $m=12$ ).



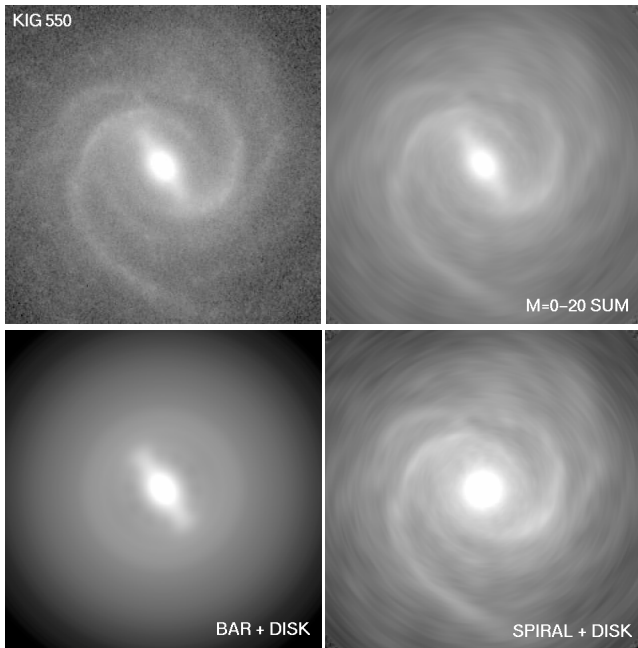


**Figure 2.** KIG 550: (*upper-left*) original reduced/deprojected i-band image; (*upper-right*) “M=0-20 SUM” image (“Fourier-smoothed” version of the original image) = the sum of the 21 Fourier terms; (*lower-left*) “BAR + DISK” image = the sum of the bar image and m=0 image; (*lower-right*) “SPIRAL + DISK” image = “M=0-20 SUM” image minus the bar image.

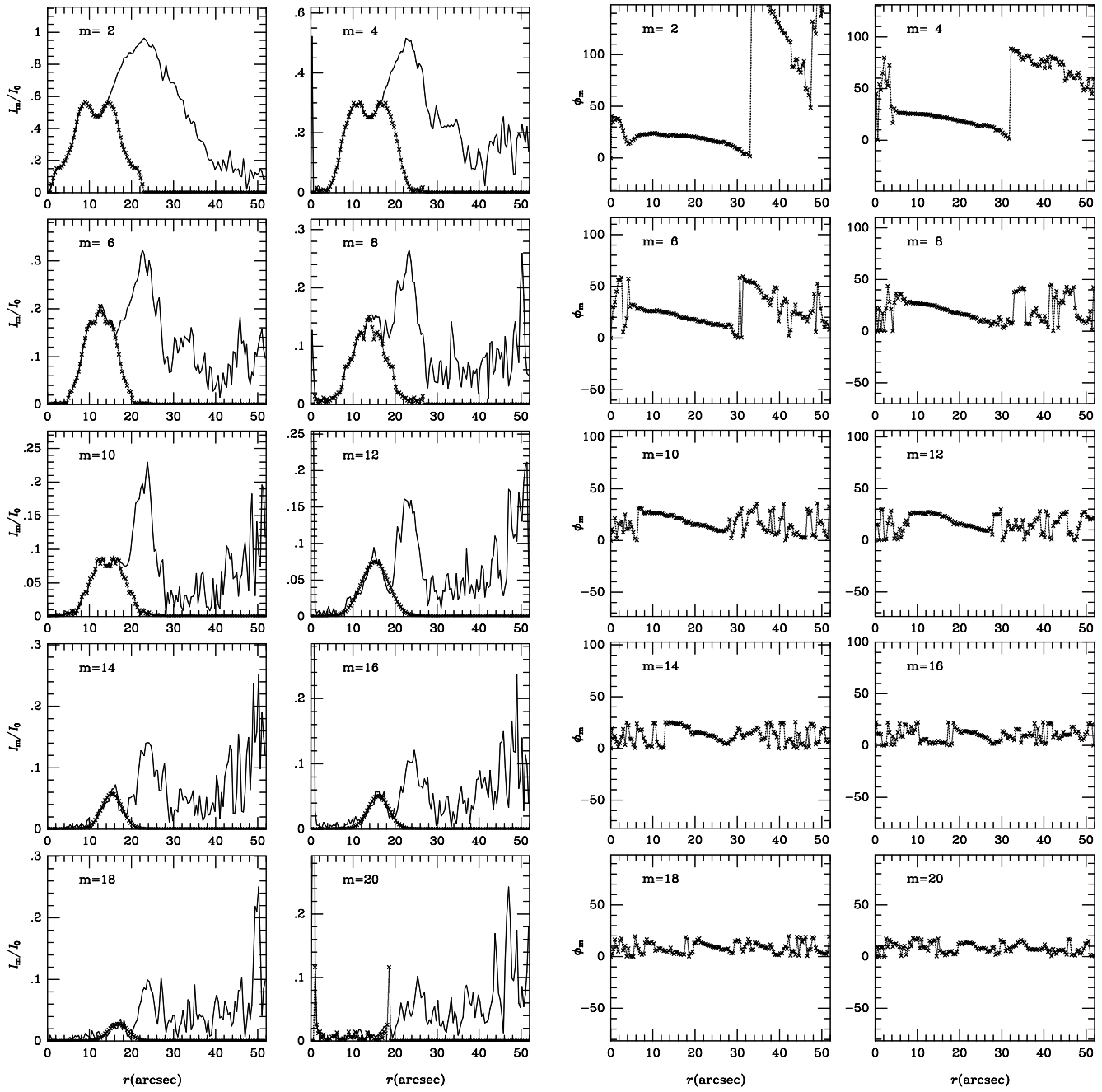


**Figure 3.** KIG 553: (*left*): Relative Fourier intensity amplitudes  $I_m/I_0$  for the first ten even Fourier terms ( $m=2$  to  $m=20$ ); (*right*): Phase profiles  $\phi_m$  for the first ten even Fourier terms ( $m=2$  to  $m=20$ ).

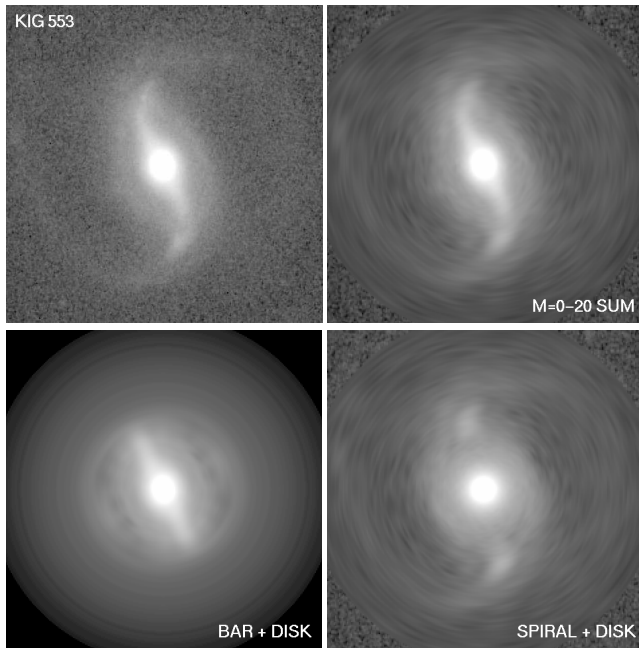


**Figure 4.** KIG 553: The designation of each image is the same as in Figure 2.

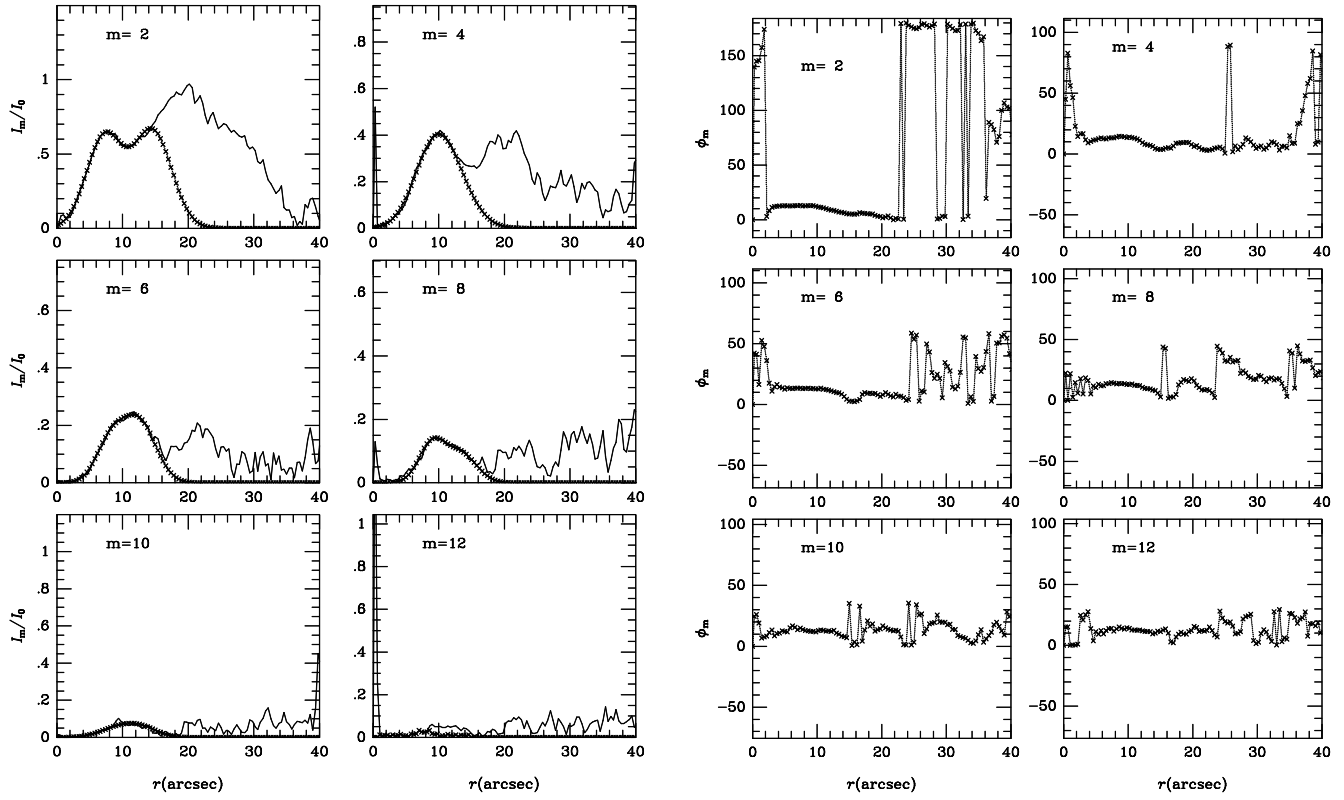


**Figure 5.** KIG 719: (*left*): Relative Fourier intensity amplitudes  $I_m/I_0$  for the first six even Fourier terms ( $m=2$  to  $m=12$ ); (*right*): Phase profiles  $\phi_m$  for the first six even Fourier terms ( $m=2$  to  $m=12$ ).

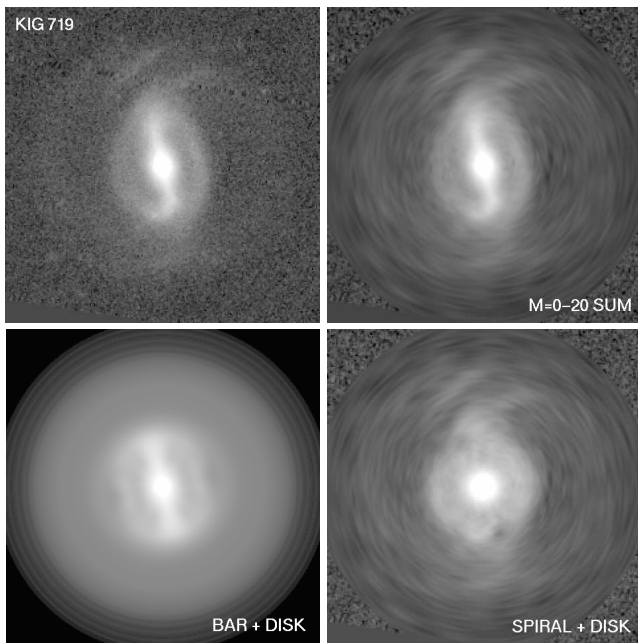


**Figure 6.** KIG 719: The designation of each image is the same as in Figure 2.

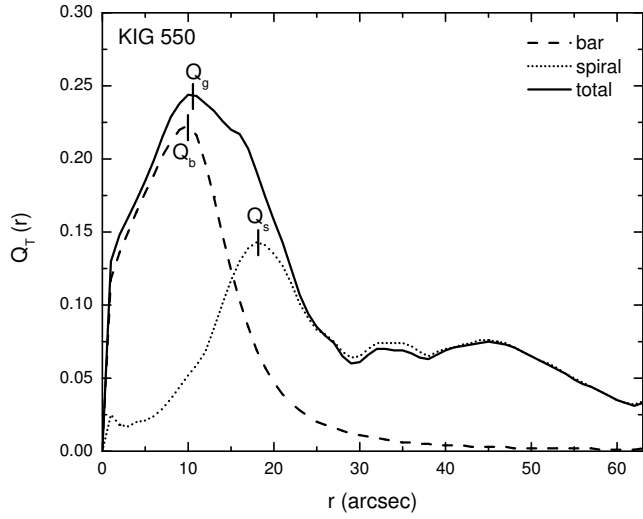


**Figure 7.** KIG 550: The relative strength of the perturbation  $Q_T(r)$  as a function of radius for the bar (dashed line), spiral structure (dotted line) and total (solid line). Bar strength ( $Q_b$ ), spiral strength ( $Q_s$ ) and total strength ( $Q_g$ ) are indicated on the figure.

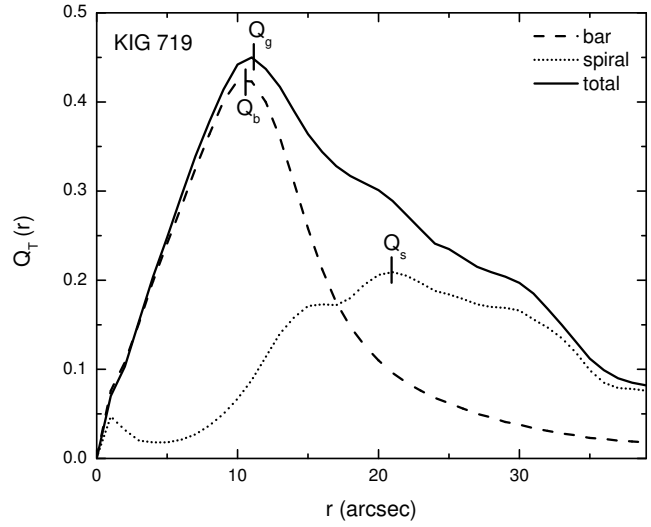


**Figure 9.** KIG 719: The relative strength of the perturbation  $Q_T(r)$  as a function of radius for the bar (dashed line), spiral structure (dotted line) and total (solid line). Bar strength ( $Q_b$ ), spiral strength ( $Q_s$ ) and total strength ( $Q_g$ ) are indicated on the figure.

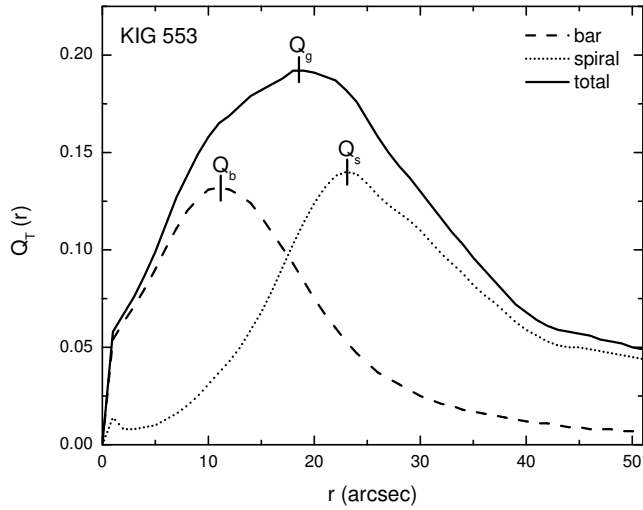


**Figure 8.** KIG 553: The relative strength of the perturbation  $Q_T(r)$  as a function of radius for the bar (dashed line), spiral structure (dotted line) and total (solid line). Bar strength ( $Q_b$ ), spiral strength ( $Q_s$ ) and total strength ( $Q_g$ ) are indicated on the figure.

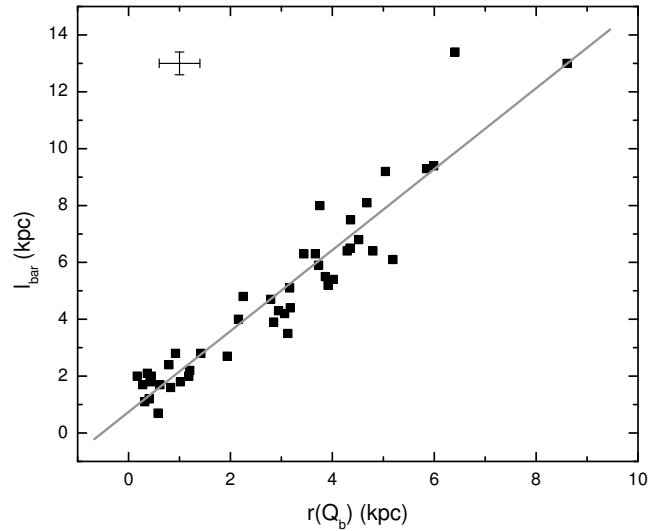


**Figure 10.** The correlation between the bar maximal torque radius  $r(Q_b)$  and the Fourier bar length  $l_{bar}$  for the CIG/KIG barred Sb-Sc galaxies in our sample (N=46). A linear regression fit of slope 1.42 is shown (correlation coefficient 0.95). The  $2\sigma$  typical error bars are shown as well.

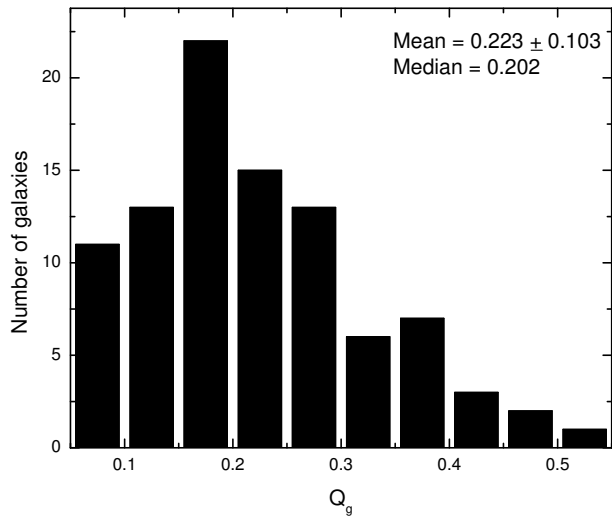


**Figure 11.** Distribution of the total strength  $Q_g$  for the CIG/KIG Sb-Sc galaxies in our sample (N=93).

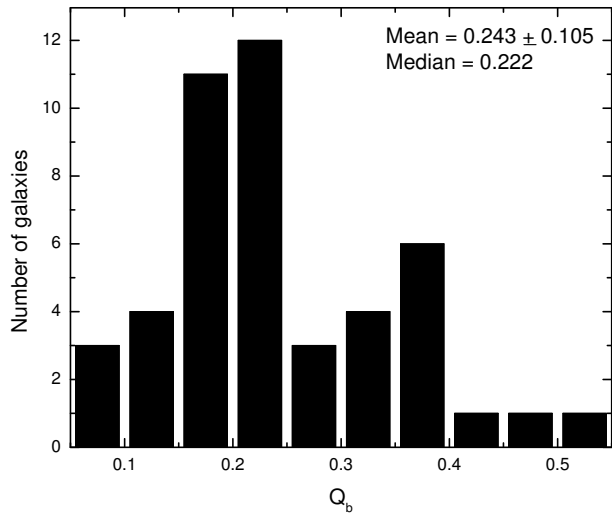


**Figure 12.** Distribution of the bar strength  $Q_b$  for the barred CIG/KIG Sb-Sc galaxies in our sample (N=46).

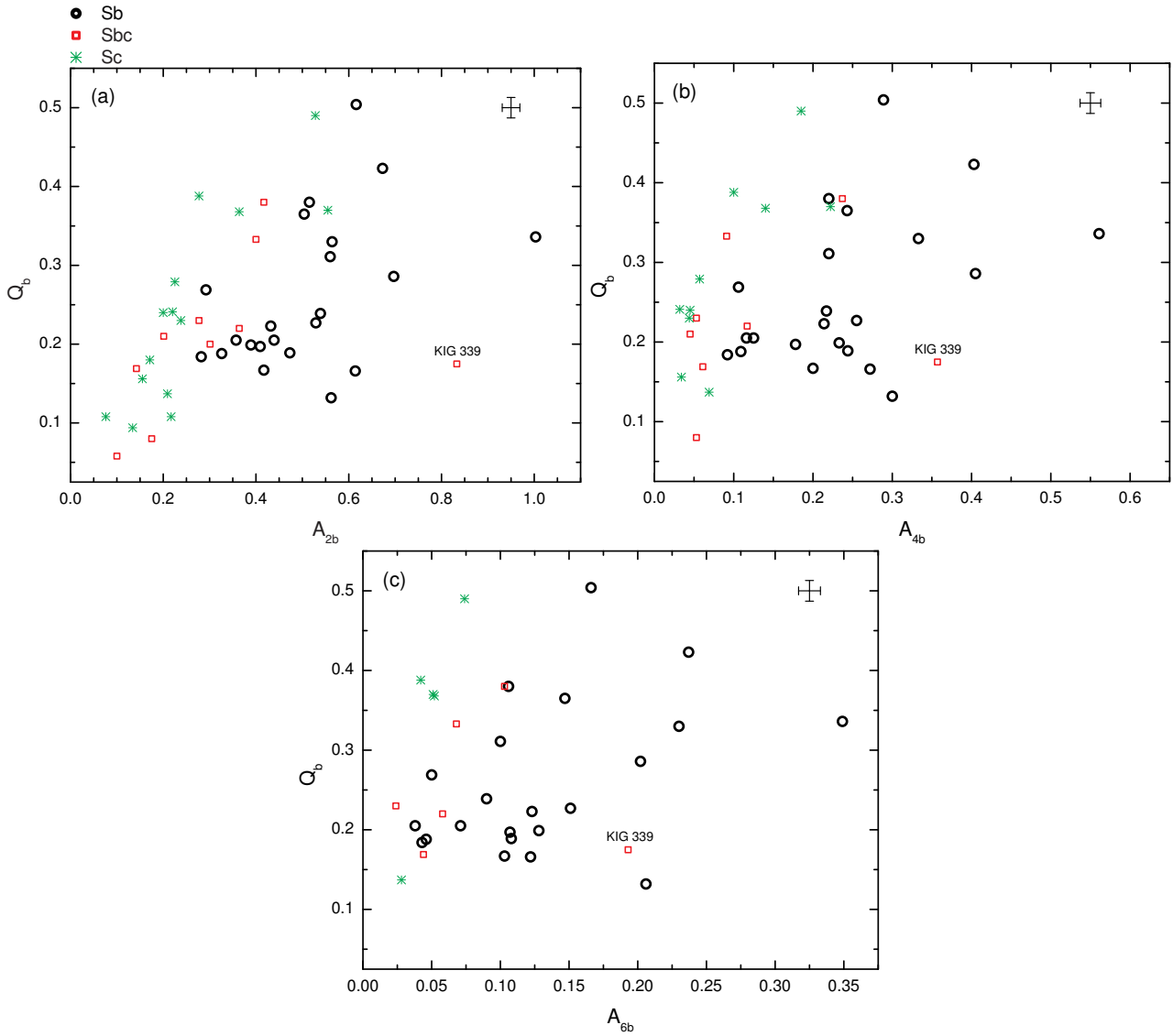


**Figure 13.** Barred CIG/KIG Sb-Sc galaxies: (a) Bar strength  $Q_b$  versus maximum relative Fourier intensity amplitudes at  $m=2$ ,  $A_{2b}$  (N=46 galaxies); (b) Bar strength  $Q_b$  versus maximum relative Fourier intensity amplitudes at  $m=4$ ,  $A_{4b}$  (N=40 galaxies); (c) Bar strength  $Q_b$  versus maximum relative Fourier intensity amplitudes at  $m=6$ ,  $A_{6b}$  (N=33 galaxies). An outlier (KIG 339) is labeled on the plots. Typical  $2\sigma$  error bars are shown in each panel.



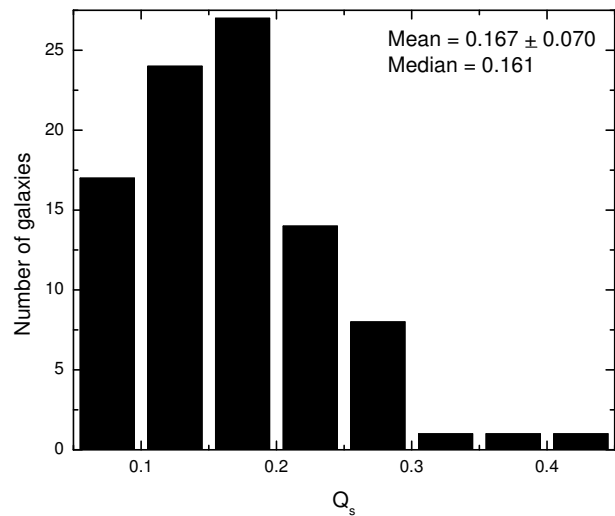


**Figure 14.** Distribution of the spiral strengths  $Q_s$  for the CIG/KIG Sb-Sc galaxies in our sample (N=93).

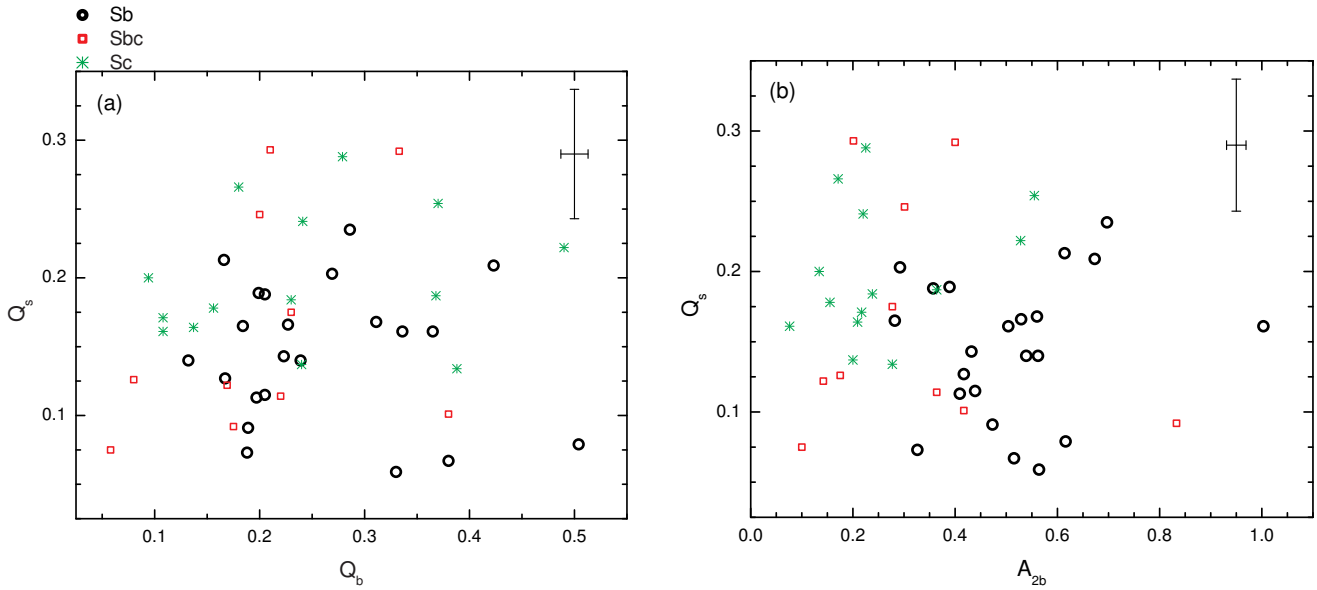


**Figure 15.** Barred CIG/KIG Sb-Sc galaxies (N=46): (a) Spiral arm strength  $Q_s$  versus bar strength  $Q_b$ ; (b) Spiral arm strength  $Q_s$  versus maximum of the relative Fourier intensity amplitudes at  $m=2$ ,  $A_{2b}$ . Typical  $2\sigma$  error bars are shown in each panel.

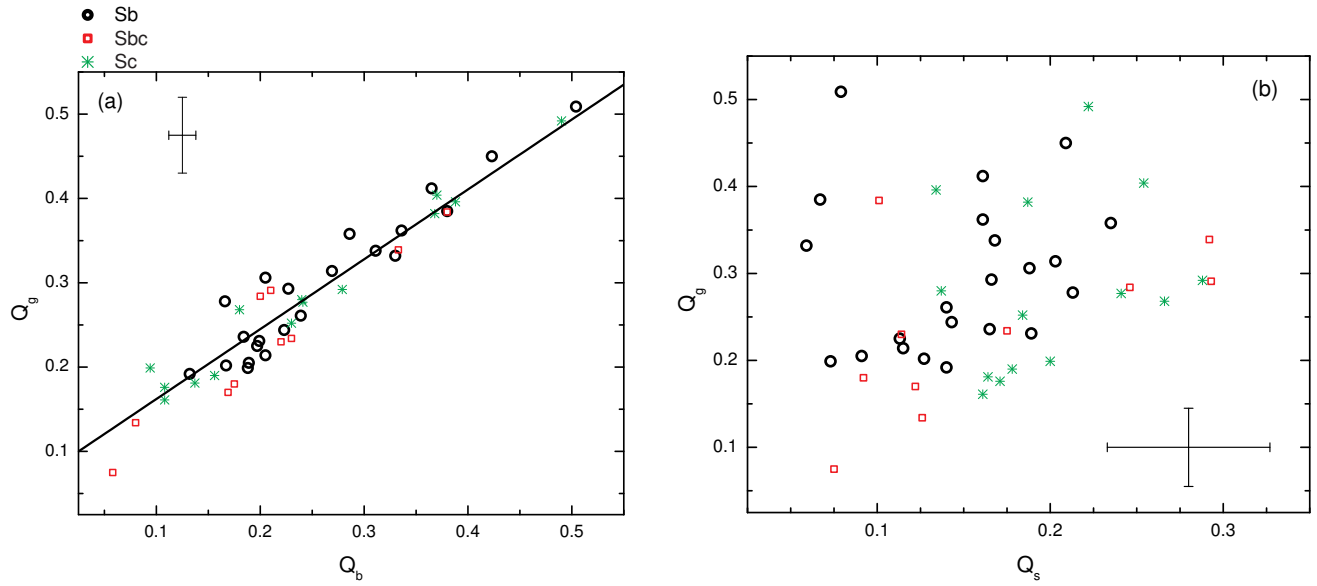


**Figure 16.** Barred CIG/KIG Sb-Sc galaxies (N=46): (a) Total strength  $Q_g$  versus bar strength  $Q_b$ ; (b) Total strength  $Q_g$  versus spiral arm strength  $Q_s$ . Typical  $2\sigma$  error bars are shown in each panel.

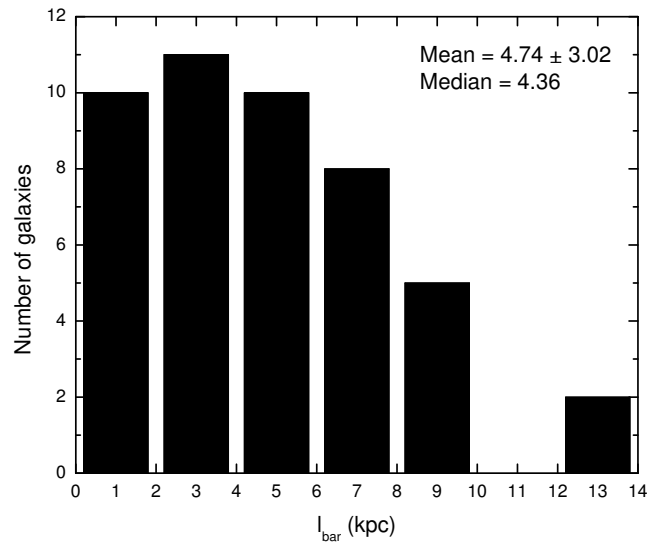


**Figure 17.** Distribution of bar sizes for barred galaxies in our sample (N=46).

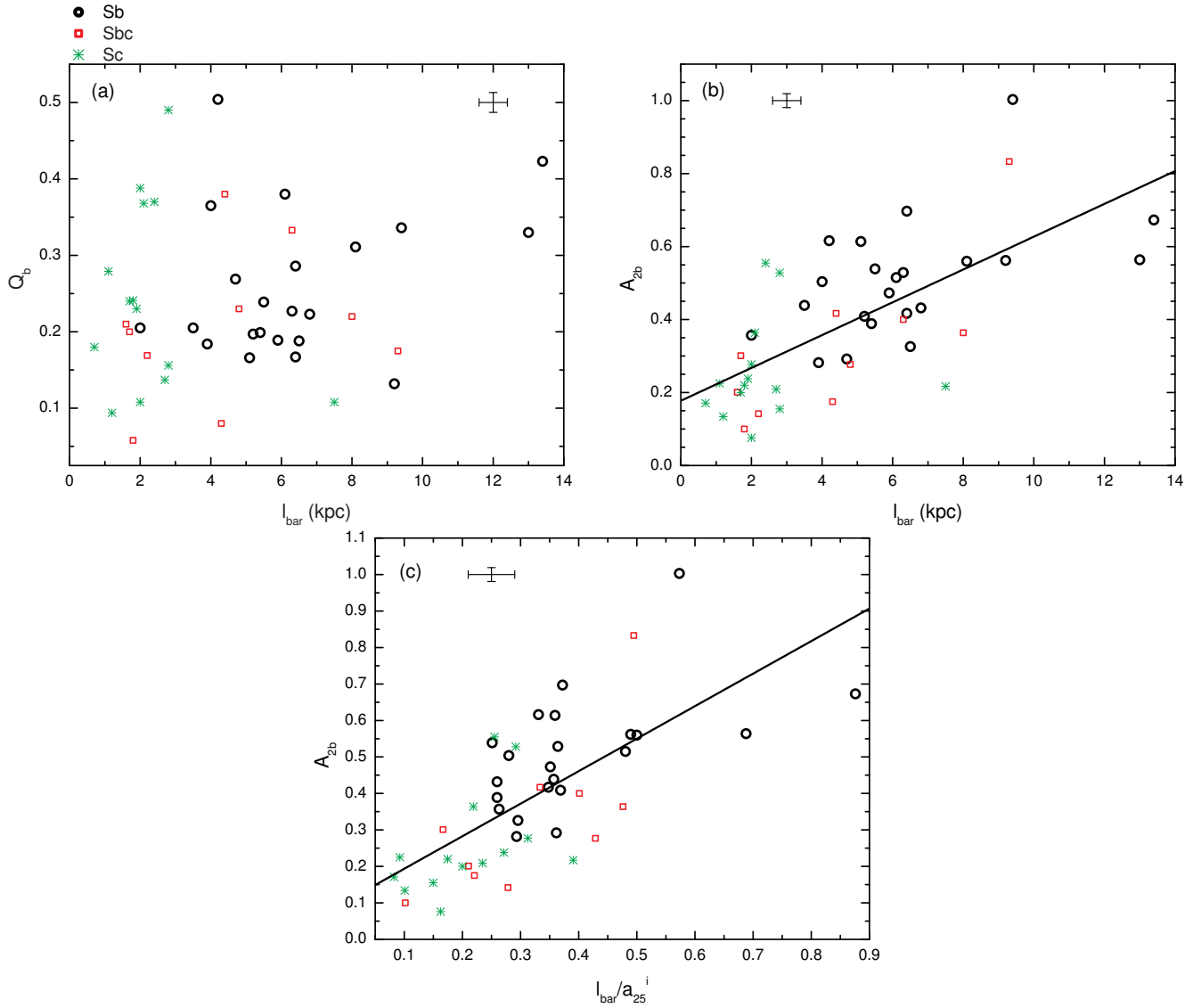


**Figure 18.** Barred CIG/KIG Sb-Sc galaxies (N=46): (a) Bar strength  $Q_b$  versus maximum of the relative Fourier intensity amplitudes at  $m=2$ ,  $A_{2b}$ . (b) Maximum of the relative Fourier intensity amplitudes at  $m=2$ ,  $A_{2b}$  versus bar size,  $l_{bar}$ . (c)  $A_{2b}$  versus bar size,  $l_{bar}$  normalized by the semimajor axis of the 25 mag arcsec $^{-2}$  isophote in i-band,  $a_{25}^i$ . Typical  $2\sigma$  error bars are shown in each panel. A linear regression is shown in panels b and c.

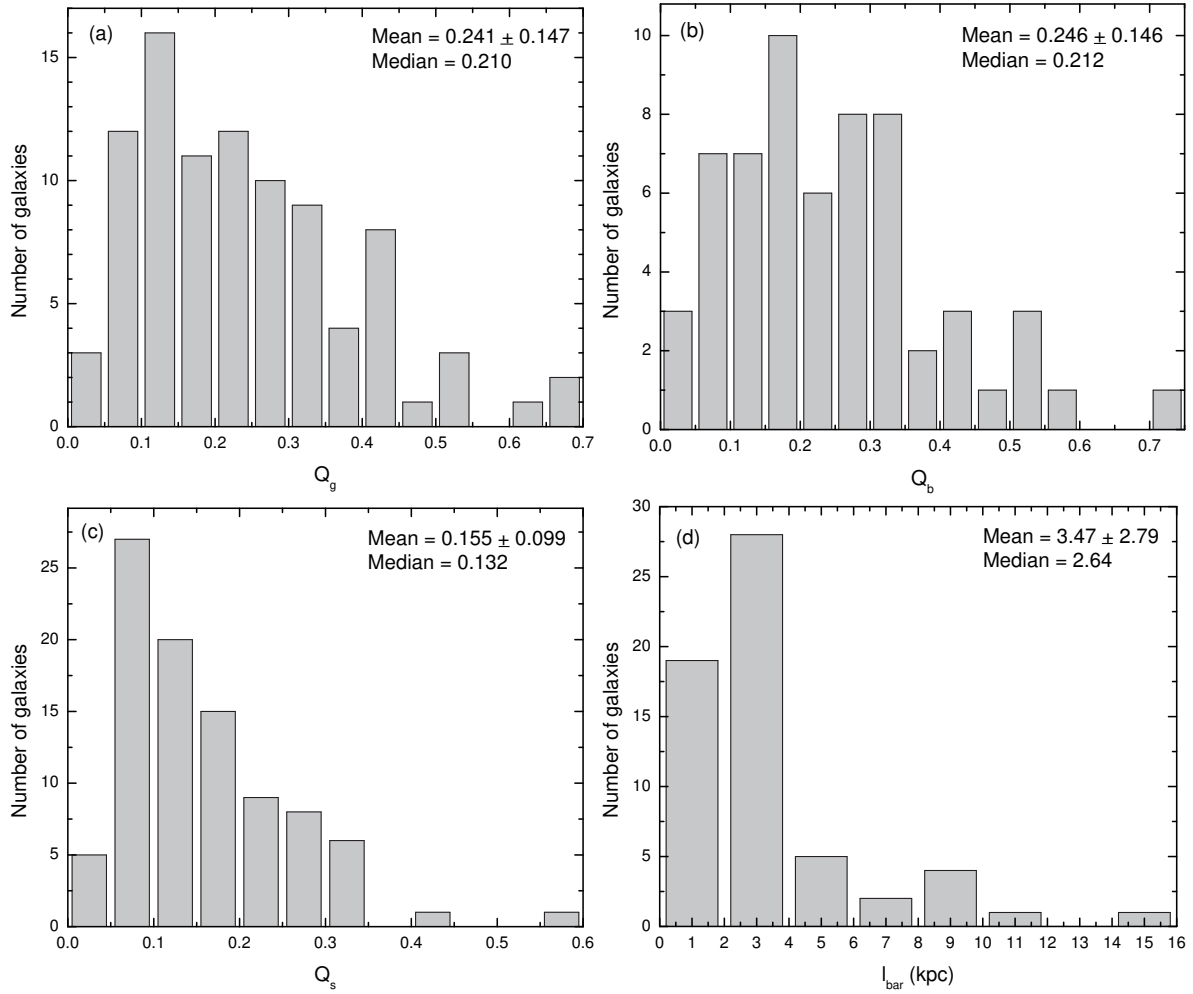


**Figure 19.** (a) Distribution of the total strength  $Q_g$  for the Sb-Sc galaxies from OSU sample (N=92); (b) Distribution of the bar strength  $Q_b$  for the barred Sb-Sc galaxies from OSU sample (N=60); (c) Distribution of the spiral strength  $Q_s$  for the Sb-Sc galaxies from OSU sample (N=92). (d) Distribution of bar sizes for barred galaxies in the OSU sample (N=60).

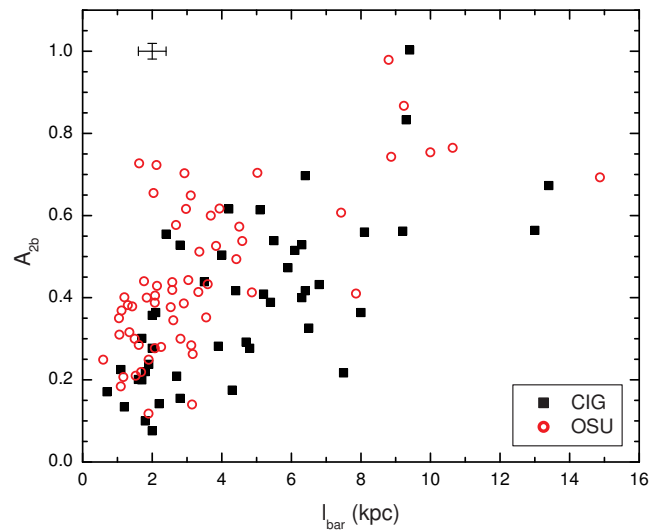


**Figure 20.**  $A_{2b}$  versus  $l_{\text{bar}}$  for the barred galaxies in our sample ( $N=46$ ) and in the OSU sample ( $N=60$ ). This shows that in near-IR bands bars can be seen in higher contrast. Typical  $2\sigma$  error bars for the CIG galaxies are shown on the figure.

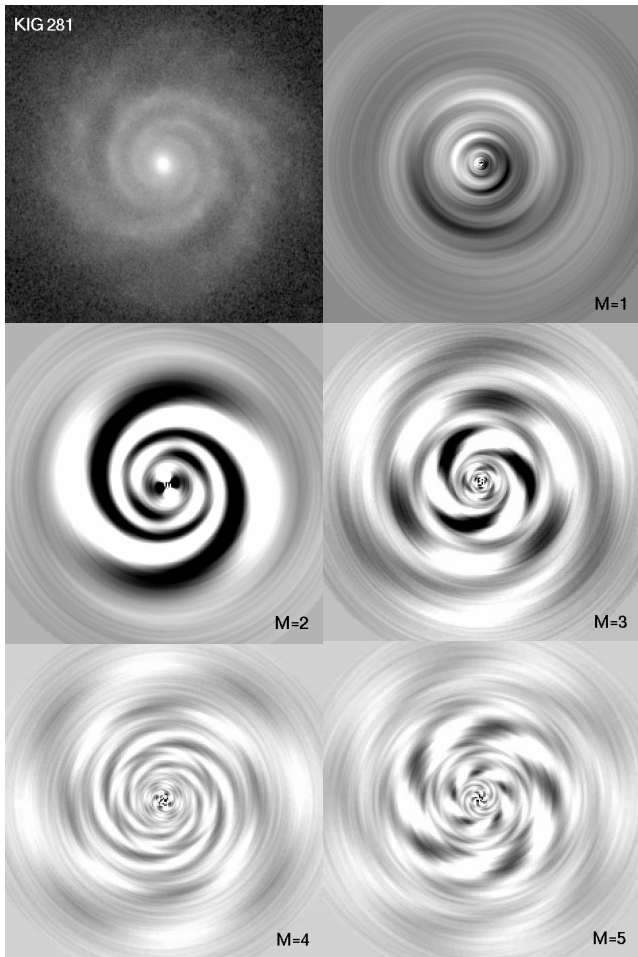


**Figure 21.** KIG 281: The original reduced & deprojected i-band image and the reconstructed  $m = 1, 2, 3, 4, 5$  Fourier term images.

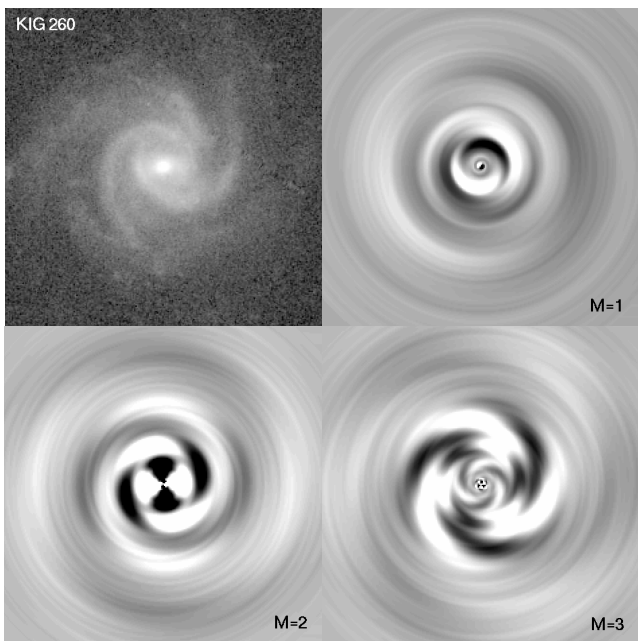


**Figure 22.** KIG 260: The original reduced & deprojected i-band image and the reconstructed  $m = 1, 2, 3$  Fourier term images.

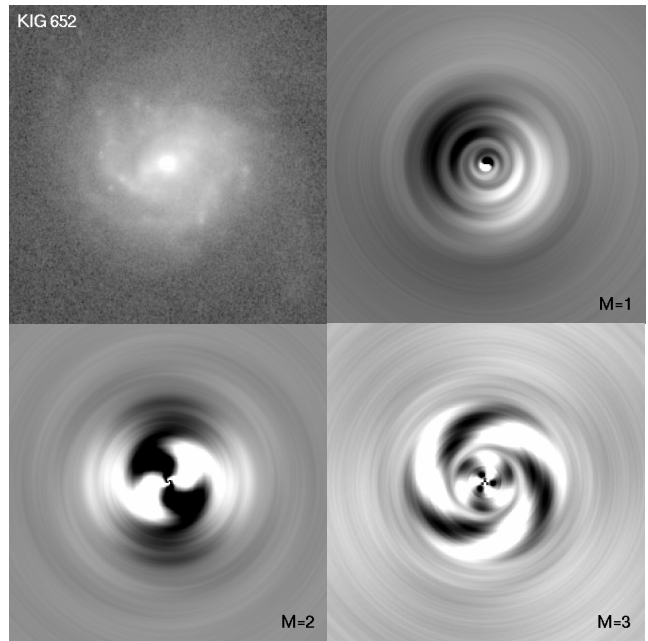


**Figure 23.** KIG 652: The original reduced & deprojected i-band image and the reconstructed  $m = 1, 2, 3$  Fourier term images.

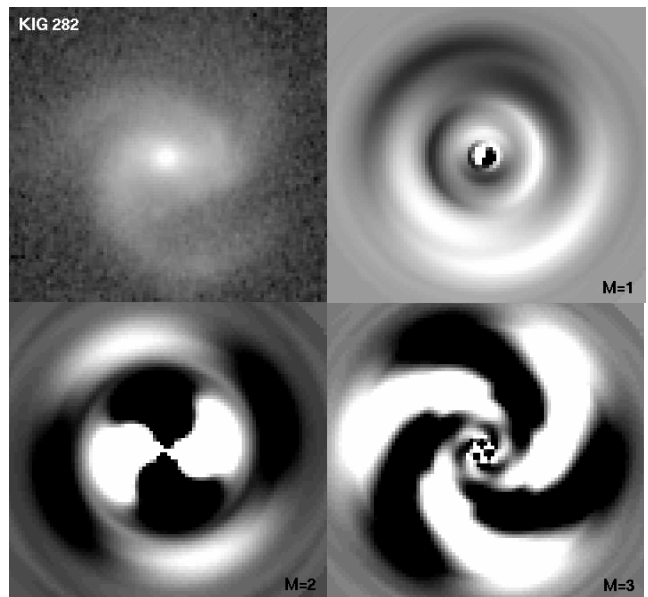


**Figure 24.** KIG 282: The original reduced & deprojected i-band image and the reconstructed  $m = 1, 2, 3$  Fourier term images.